Materials Advances

ROYAL SOCIETY OF CHEMISTRY

PAPER

View Article Online
View Journal | View Issue

Cite this: *Mater. Adv.*, 2025, **6**, 6787

Impact of composition on the structural, electronic, and mechanical properties of $M_3C_2T_2$ MXenes

Emily Sutherland,[a] Benjamin Traverso[b] and N. Aaron Deskins*[b]

MXenes are a family of layered 2D materials useful for a wide variety of applications. Their properties can be fine-tuned by choice of chemical composition (metal and termination), but the vast majority of published studies have focused on Ti-based MXenes with –O, –F, and –OH terminations. Furthermore, MXenes may have ABC or ABA stacking, but typical density functional theory (DFT) studies assume only ABC stacking. Thus, most modeling papers of MXenes have focused only on specific targeted MXenes. In this work we aimed to provide a comprehensive DFT study of possible MXenes in order to motivate and characterize MXenes beyond those common in the literature. We modeled 99 different $M_3C_2T_2$ MXenes (including group 4, 5, and 6 metals; also including halogen, chalcogen, –OH, and –NH terminations). We made no assumptions about preferred termination site or stacking symmetry of these MXenes. 20% of the studied MXenes were found to prefer ABA stacking. In total we performed more than 2000 DFT calculations to predict the structural, electronic, and mechanical properties of these MXenes. We identified several MXenes with exceptional properties, and identified potential applications of such MXenes. We also connected the termination/metal choice to trends in their properties. Our work highlights how different properties of MXenes can be tuned based on their composition, and thus motivates further work on these materials.

Received 8th August 2025,
Accepted 12th August 2025

DOI: 10.1039/d5ma00874c

rsc.li/materials-advances

1 Introduction

In recent years MXenes have attracted much attention due to their potential tunability and unique properties.[1–5] They have been studied for many applications, including energy storage,[6–11] photocatalysis,[12–15] electrocatalysis,[16–20] electronic devices,[21–23] sensing,[24–27] and others. MXenes are two-dimensional materials that have the chemical formula $M_{n+1}X_nT_x$, where M is an early transition metal, X is C or N, and T is a surface termination. The number of layers (n) is typically 1 to 4.[28] The termination can have a profound role on the MXene properties,[29,30] for instance making it a metal or semiconductor depending on the termination,[31–34] or changing mechanical properties.[35–37] Other properties, such as work function[38–42] can also change depending on the constituent components (M, X, or T). Understanding and predicting MXene properties based on their composition and structure is a critical part of advancing applications of these materials.

Most commonly, MXenes are synthesized from MAX phase materials where the A layer is removed *via* aqueous acids (*e.g.*, HF), resulting in –F, –O, and/or –OH terminations.[43,44] Still, other terminations on MXene surfaces are possible.[29,30,45–47] For instance, electrochemical etching or using Lewis acidic molten salts may produce –Cl, –Br, –I, –P, or –Sb terminations.[48–52] Furthermore, through post-processing of MXenes it is possible to remove terminations (producing bare MXenes) or substitute existing terminations with a new termination, such as –S, –Se, –Te, or –NH.[49,53] Despite efforts to make MXenes having various compositions, it has been estimated that around 80% of published MXene papers have focused on Ti-based MXenes.[54,55] Even papers with a theoretical component are also predominantly focused on Ti-based MXenes.[55] Furthermore, density functional theory (DFT) studies often tend to focus on n = 1 MXenes.[31,34,35,56–59] Ignoring $Ti_3C_2T_2$ and Ti_2CT_2 (which are the most commonly studied MXenes), papers with a theoretical component and focused on n = 1 MXenes are around 20 times more common than papers with a theoretical component and focused on n = 2 MXenes.[55] Accordingly, more data and understanding of MXenes beyond those commonly studied (*e.g.*, metals other than Ti and $n > 1$) is needed in order to achieve the goal of fully tuning MXenes for targeted applications.

There have been several DFT studies performed examining the impact of different surface terminations on the properties of MXenes. Much of this work however has focused on –O, –OH,

[a] *Department of Physics, Worcester Polytechnic Institute, Worcester, Massachusets, USA. E-mail: egsutherland@wpi.edu*
[b] *Department of Chemical Engineering, Worcester Polytechnic Institute, Worcester, Massachusets, USA. E-mail: nadeskins@wpi.edu*

or –F terminations for various metals.[11,31,35,40,58–66] O-terminated MXenes generally have higher mechanical strength[35,60] and are more likely to be semiconductors[28,35,58] compared to those with –F or –OH terminations. Terminating a MXene with OH groups tends to result in an ultralow work function.[38–40,60,65] While there are studies which model halide (F, Br, Cl, I) or chalcogen (O, S, Se, Te) terminated Ti_2CT_x and $Ti_3C_2T_x$ MXenes,[42,67–71] studies modeling terminations other than –O, –F, and –OH for MXenes with metals other than Ti- are limited.[40,71–78] In addition, many MXenes have ABC stacking,[79,80] but it is possible that the atomic layers may have ABA stacking.[81,82] Theory predicts ABA stacking for certain MXenes.[34,66,80,83–85] Despite this, the vast majority of DFT studies on MXenes assume ABC stacking, or ignore the possibility of ABA stacking. Thus far, DFT studies comparing ABA and ABC stacking have been reported for bare MXenes[34,80,84,85] and for those with –O,[34,66,75,80,84] –F,[66,75,84] –OH,[66] –S,[75] –Cl,[75] or –P[83] terminations. Thus, there is a need for more simulation data on non-Ti MXenes, as well as identifying the right stacking (in order, for instance, to correctly model these MXenes) for MXenes with other termination and/or metal combinations.

In this work we modeled 99 carbide MXenes (*i.e.*, $M_3C_2T_2$), including 9 metals (groups 4, 5, and 6) and 10 possible terminations (halogens, chalcogens, OH, and NH). Our goal was to provide a comprehensive analysis of how metal and termination choice affects the structural stability and other properties of the MXenes. The literature on DFT modeling of MXenes has largely focused on a small subset of MXenes (typically Ti-based; or M_2CT_x MXenes, $n = 1$), or a small subset of properties. Many literature papers have also assumed ABC stacking for MXenes. Our work represents the most comprehensive DFT study of $M_3C_2T_2$ ($n = 2$) MXenes involving a wide range of metals and terminations, and this many structural, electronic, and mechanical properties. Fig. 1 highlights the MXenes that we modeled, as well as the properties we calculated. In order to determine the correct stable structures, we modeled both ABC and ABA stacking for each MXene. We also considered four possible surface sites for terminations. We then report several properties for each of the most stable configurations, including electronic and mechanical properties. By identifying, examining, and analyzing the observed trends, we indicate how MXene properties can be controlled through their chemical composition, and which MXenes have promising properties.

2 Methodology

We performed DFT calculations using the Vienna ab initio Simulation Package (VASP).[86–89] The exchange correlation energy was calculated using the generalized gradient approximation (GGA) functional by Perdew, Burke, an Ernzerhof (PBE).[90] Core electrons were described by projector augmented wave (PAW) pseudopotentials.[91,92] A cutoff energy of 450 eV was used for valence electron wavefunctions. As recommended by the VASP developers, we utilized the following number of valence electrons for each metal: Ti (12), Zr (12), Hf (10), V (13), Nb (13), Ta (11), Cr (12), Mo (14), and W (14). The Brillouin zone was sampled with a Γ-centered $8 \times 8 \times 1$ k-point mesh. Calculation convergence criteria for the energies and forces were set to 10^{-5} eV and 0.002 eV Å^{-1}, respectively. We used the Gaussian smearing method with a width 0.25 eV, which was found to minimize roughness in density of states (DOS) plots while retaining principle features. One goal of examining the electronic structure was to identify any semiconductors (MXenes are predominantly metallic). The PBE functional is known to underestimate band gaps, so electronic structures were also calculated using the HSE06 functional.[93] HSE06

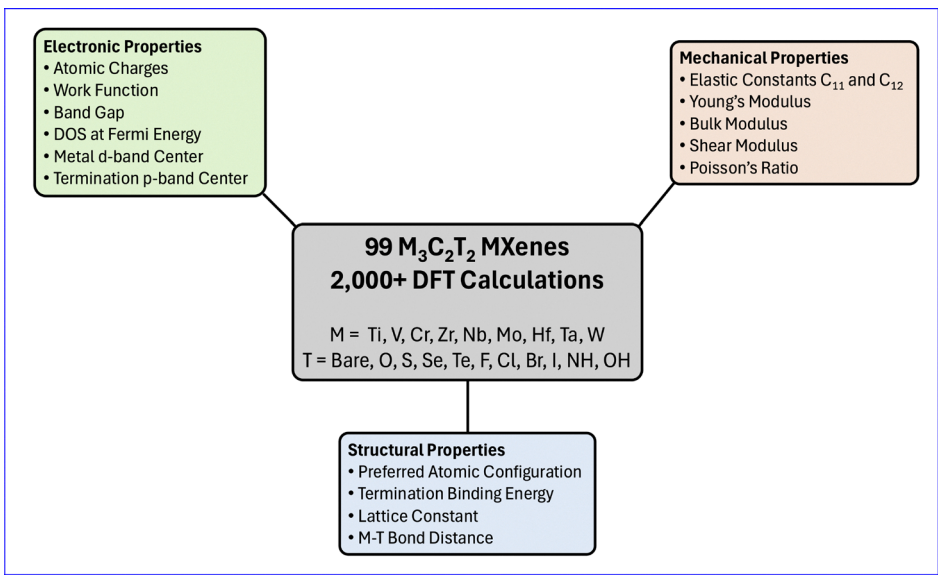

Fig. 1 Illustration of the MXenes modeled in this work, and the various calculated properties. This work contains the most comprehensive DFT study to date which has modeled $M_3C_2T_2$ ($n = 2$) MXenes and the listed properties.

provides a more accurate way to verify whether a MXene is a semiconductor. Since we were primarily interested in identifying semiconductors with the HSE06 functional, for these calculations we used a smearing width of 0.05 eV, as recommended by the VASP developers for semiconductors. Identifying band gaps from DOS plots can be challenging, especially since smearing in the DOS increases overlap of electronic states and band gaps will depend on the smearing width. Identifying band gaps is also ambiguous from DOS plots since band edges are arbitrarily defined in the plots. All reported band gaps are therefore taken from the electronic eigenvalues, rather than DOS plots.

Post-processing of DOS data was performed using the VASPKIT package.[94] Bader charge analysis was performed using code from the Henkelman group.[95] Two-dimensional elastic properties were calculated using the energy-strain method as implemented in VASPKIT.[94,96] In calculating the elastic properties, we considered strain along the x and y axis to range from -0.015 to 0.015 ε in steps of 0.005 ε. We also calculated MXene d-band centers as the first moment of the projected DOS for the metal atom d-bands.[97,98] Due to the small thickness of the MXenes, we included the d-bands of all metal atoms in our calculations, rather than considering surface metal atoms only. Previous literature[99–101] integrated the DOS from $-\infty$ to a finite positive value in order to capture all relevant d-band orbitals. Similarly, based on inspection of our DOS, we integrated the d-bands from $-\infty$ to 2 eV. All structural visualizations were carried out using VESTA.[102]

Correlation coefficients provide a simple way to investigate relationships between MXene properties and properties of their constituent atoms. Therefore, we calculated Pearson correlation coefficients between various MXene properties and elemental properties (as reported in the Mendeleev[103] database). Correlation coefficients were found using the Orange Data Mining program.[104] A more extensive investigation of these relationships using statistical methods will be the focus of future work.

We modeled monolayer M_3C_2 and $M_3C_2T_2$ MXenes with M = Ti, Zr, Hf, V, Nb, Ta, Cr, Mo, and W (groups 4, 5 and 6), and T = O, S, Se, Te, F, Cl, Br, I, OH, and NH (including chalcogens and halogens). All MXenes were modeled at full coverage, which is expected to have higher thermodynamic stability compared to lower coverages.[31] To avoid interactions between neighboring monolayers, our calculations included a cell length of 22 Å in the z-direction, which gave vacuum distances of at least $\approx$12 Å for terminated surfaces. We modeled both trigonal (ABC) and hexagonal (ABA) stacking symmetry (shown in Fig. 2) for all the MXenes. Additionally, there are multiple high-symmetry sites where terminal groups may attach to the MXene surface. Previous literature identified several possible stable termination sites.[11,31,35,58–60,78] These include hollow sites above metal atoms (hM), hollow sites above no atoms (h), hollow sites above X layer atoms (hX), mixed sites with hM or h on one surface and hX on the other (m), and directly on top of metal atoms (t). Fig. 2 shows side views of the different termination sites along with stacking configurations. In total we modeled 8 configurations for each terminated MXene (four termination sites and two stacking arrangements). Side and top views of all the different configurations are shown in Fig. S1 and S2.

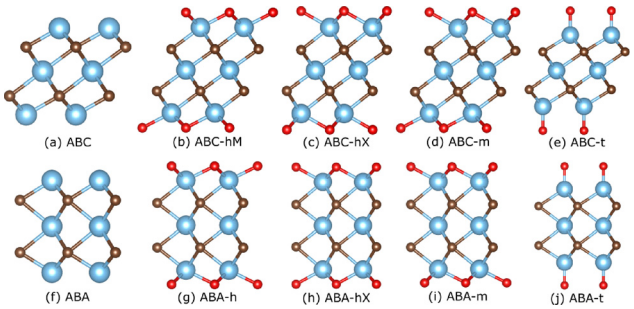

Fig. 2 Different MXene configurations modeled in this work. Blue spheres represent metal atoms, brown spheres represent carbon atoms, and red spheres represent terminating atoms. MXenes were modeled with trigonal (ABC) stacking (a)–(e) or hexagonal (ABA) stacking (f)–(j). ABC terminations are designated as follows: hollow sites above metal atoms (hM), hollow sites above carbon (hX), mixed termination sites with one surface hM and one surface hX (m), and top sites (t). ABA terminations are designated as follows: hollow sites between metal and carbon (h), hollow sites above carbon (hX), mixed termination sites with one surface h and one surface hX (m), and top sites (t). Top views of the structures can be found in Fig. S1 and S2 in the SI.

3 Results and discussion

3.1 Structural properties

3.1.1 Preferred stacking and termination sites. We first identified the most stable structures for each MXene, especially to understand how the composition affects the preferred MXene geometry. In Fig. 3, and in (Tables S1, S2 and Fig. S3, S4), we report the most stable structures and relative energy values comparing different stacking configurations and sites for each termination. Our results showed that, while the majority of M_3C_2 and $M_3C_2T_2$ MXenes displayed an energetic preference for ABC stacking, some MXenes were more stable with ABA stacking. In total, 20% of the modeled MXenes were more stable with ABA stacking, which is not trivial. A statistical summary of the most stable configurations and terminations is found in Fig. S3.

We report energy differences between ABA and ABC stacking configurations ($\Delta E_{ABA-ABC} = E_{ABA} - E_{ABC}$) for each bare MXene in Table S1. We found that all bare MXenes containing group 4 metals (Ti, Zr, Hf) had a strong energetic preference for ABC stacking, with an average $\Delta E_{ABA-ABC}$ value of 2.72 eV. We also found that bare MXenes with group 5 metals (V, Nb, Ta) had an energetic preference for ABC stacking, with an average $\Delta E_{ABA-ABC}$ value of 1.85 eV. On the other hand, bare MXenes with group 6 metals (Cr, Mo, W) preferred ABA stacking, with negative $\Delta E_{ABA-ABC}$ values for Mo_3C_2 (-0.30 eV) and W_3C_2 (-1.13 eV). Bare Cr_3C_2 had a $\Delta E_{ABA-ABC}$ of 0.11 eV, which indicated that it may be stable with either ABC or ABA stacking. Gouveia *et al.*[80] also found similar results for bare MXenes.

The most stable structures from the eight considered configurations (see Fig. 2) are reported in Fig. 3 and Fig. S4 for each $M_3C_2T_2$ MXene. We found that all terminated MXenes with

	$Ti_3C_2T_2$	$V_3C_2T_2$	$Cr_3C_2T_2$
Bare	ABC	ABC	ABC
O	ABC-hM	ABC-hM	ABA-hX
S	ABC-hM	ABC-hM	ABA-hX
Se	ABC-hM	ABC-hM	ABC-hX
Te	ABC-hM	ABC-hM	ABC-hM
F	ABC-hM	ABC-hX	ABC-hM
Cl	ABC-hM	ABC-hM	ABC-hM
Br	ABC-hM	ABC-hM	ABC-hM
I	ABC-hM	ABC-hM	ABC-hM
NH	ABC-hM	ABC-hM	ABA-hX
OH	ABC-hM	ABC-hX	ABC-hM

	$Zr_3C_2T_2$	$Nb_3C_2T_2$	$Mo_3C_2T_2$
Bare	ABC	ABC	ABA
O	ABC-hM	ABC-hM	ABA-hX
S	ABC-hM	ABC-hM	ABA-hX
Se	ABC-hM	ABC-hM	ABA-hX
Te	ABC-hM	ABC-hM	ABC-m
F	ABC-hM	ABC-hX	ABA-h
Cl	ABC-hM	ABC-hX	ABA-h
Br	ABC-hM	ABC-hX	ABC-hM
I	ABC-hM	ABC-hM	ABC-t
NH	ABC-hM	ABC-hX	ABA-hX
OH	ABC-hM	ABC-hX	ABA-m

	$Hf_3C_2T_2$	$Ta_3C_2T_2$	$W_3C_2T_2$
Bare	ABC	ABC	ABA
O	ABC-hM	ABC-hM	ABA-hX
S	ABC-hM	ABC-hM	ABA-hX
Se	ABC-hM	ABC-hM	ABA-hX
Te	ABC-hM	ABC-hM	ABA-hX
F	ABC-hM	ABC-hX	ABA-h
Cl	ABC-hM	ABC-hX	ABA-h
Br	ABC-hM	ABC-hX	ABC-t
I	ABC-hM	ABC-hM	ABC-t
NH	ABC-hM	ABC-hM	ABA-hX
OH	ABC-hM	ABC-hX	ABA-m

Fig. 3 Indication of the most stable stacking and termination sites for each MXene, as determined by calculated energies. MXenes which prefer ABC stacking are shown in blue shades, while MXenes which prefer ABA stacking are shown in green shades. 20% of the studied MXenes preferred ABA stacking.

group 4 metals showed an energetic preference for ABC stacking, regardless of termination, and also all preferred the ABC-hM configuration. Similarly, all terminated MXenes with group 5 metals also showed an energetic preference for ABC stacking, with the majority of MXenes preferring ABC-hM. However, several MXenes preferred the ABC-hX configuration over ABC-hM (*e.g.*, $V_3C_2T_2$ with –F and –OH terminations; $Nb_3C_2T_2/Ta_3C_2T_2$ with –F, –Cl, –Br, and –OH terminations; $Nb_3C_2(NH)_2$). In the ABC-hX configuration, C and T atoms are in alignment for increased steric and/or Coulombic repulsion, while such repulsion is minimized with the ABC-hM configuration. This is typically cited as the reason ABC-hM is preferred over ABC-hX.[11,34,70,105]

Several MXenes involving group 6 metals were more stable with ABA stacking. Furthermore, several MXenes with group 6 metals had a near degeneracy between ABC and ABA configurations (see Fig. S4) which is in contrast to the distinct preference for ABC stacking shown by MXenes with group 4 or 5 metals. For Cr-based MXenes, ABC stacking is the dominant configuration, but some terminations induce ABA stacking (*e.g.*, O, S, NH). A shift occurs with Mo- and W-based MXenes, where an even larger number of MXenes prefer ABA stacking. All but the largest terminations (*e.g.*, –Br, –I) led to ABA stacking being preferred over ABC stacking. Gouveia *et al.* also found that $M_3C_2O_2$ MXenes with group 6 metals prefer ABA stacking, but did not model terminations other than –O.[80]

It has been shown in previous work on other layered materials, that the electron count of the material may be predictive of the energetically preferred structure.[66,106,107] Electron count is defined as the number of valence d electrons remaining on each metal atom after charge transfer to non-metal atoms.[107] For example, $Ti_3C_2F_2$ has three Ti atoms (each with four valence d electrons), two C atoms (each requiring four electrons to fill their outer shell), and two F atoms (each requiring one electron to fill their outer shell). The electron count per metal atom for $Ti_3C_2F_2$ is then $[(3)(+4) + (2)(-4) + (2)(-1)]/3 = 0.6\ e^-$ per M. Electron count is given for each bare MXene in Table S1 and for each atomic terminated MXene in Table S2.

We found that MXenes with group 6 metals had the highest electron counts (3.33 e^- per M for bare; $\geq$ 2 e^- per M for terminated) and were the only metals which had any preference for ABA over ABC stacking. This supports the argument by Gouveia *et al.*[80] that higher electron density (for instance as caused by more d electrons) leads to stronger ABA preference. For bare MXenes, $\Delta E_{ABA-ABC}$ values followed this trend for the group 6 metals: Cr > Mo > W. Correspondingly, the total number of electrons follows this trend: Cr < Mo < W, which further confirms the idea that more electron density may favor ABA stacking.

For terminated MXenes, we also found a relationship between the electron count and stacking/termination preferences. In addition to electron count, the relative sizes of atoms in a crystal are known to be a determining factor for structural preference in materials.[106,108] For example, the Goldschmidt tolerance factor and the ionic filling fraction can be used to predict the structure of perovskites and other materials.[109] We define $V_{M/T}$ as the ratio of atomic volume of the metal atom to atomic volume of the termination atom. Values of $V_{M/T}$ are provided in Table S2, utilizing atomic volume data from the Mendeleev database.[103] We summarized our findings on the preferred stacking and termination sites in Fig. 4. This shows how the electron count and relative sizes of the metal to termination are key to the preferred stacking and termination site. We also indicate in this graphic the local geometry of the termination/metal sites, as exhibited in Fig. S5. Those MXenes with smaller electron count and/or smaller $V_{M/T}$ ratios tend to

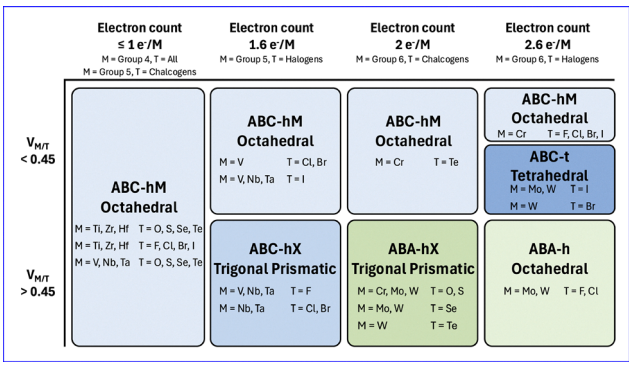

Fig. 4 A summary of our findings on the preferred stacking, preferred termination, and preferred local geometry, as they relate to electron count and $V_{M/T}$.

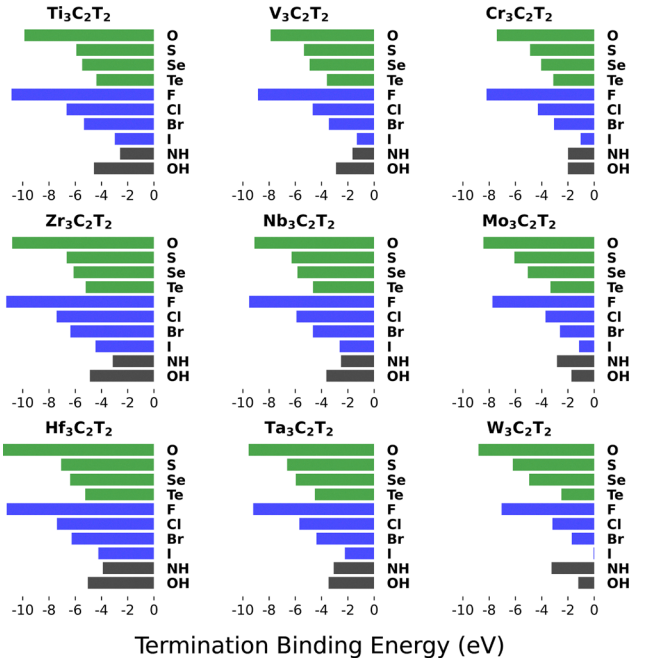

Fig. 5 Termination binding energies (eV) for terminated MXenes in their most stable configurations. Green lines are chalcogen terminated, blue lines are halogen terminated, and black lines are –NH and –OH terminated.

prefer ABC stacking (*e.g.*, group 4 or 5 metals; group 6 metals with large terminations). On the other hand those MXenes with an electron count of ≥ 2 e$^-$ per M and large $V_{M/T}$ ratios (*e.g.*, group 6 metals with O or S) preferred ABA stacking. Thus, we have uncovered an important relationship for predicting the energetically preferred configuration of MXenes.

3.1.2 Termination binding energies. We next predicted the binding energy (E_B) of the terminations, which is the energy to bind the terminations to bare MXenes. These values are useful for comparing the stability of different terminations, since one can directly compare how much energy is released (or required) to terminate a bare MXene with a given termination. The difference in binding energies of two different terminations provides the energy released or required to exchange the terminations (*i.e.*, $E_{\text{B-termination1}} - E_{\text{B-termination2}} < 0$ implies termination 1 is more stable on the surface compared to termination 2). For atomic terminated MXenes, we calculated the binding energy according to eqn (1)

$$E_B = E_{M_3C_2T_2} - E_{M_3C_2} - E_{T_2}. \quad (1)$$

Here $E_{M_3C_2T_2}$, $E_{M_3C_2}$, and E_{T_2} are, respectively, the energies of the most stable terminated MXene, the bare MXene, and the gas-phase dimer of the terminating element.[31,72,110,111] The Supplementary Information describes how binding energies of –OH and –NH terminations were calculated. The calculated binding energies are given in Fig. 5 and Table S3.

Our results showed that the most stable terminations were either –O or –F, having average binding energies of −9.26 and −9.32 eV, respectively. Other terminations were notably less stable compared to –O and –F. For instance, the average binding energy for –S (third most stable termination) was 3.15 eV less stable than –O and 3.21 eV less stable than –F. Generally, chalcogen terminations were more stable than halogen terminations (with the exception of –F), and the binding energies within a group weakened as the termination valence electrons occupied larger shells (*i.e.*, moving down the periodic table). Our results showed that metals with a higher number of valence d electrons tended to have weaker binding energies (*e.g.*, $E_{\text{B-Cr}_3C_2T_2\text{-avg}} > E_{\text{B-V}_3C_2T_2\text{-avg}} > E_{\text{B-Ti}_3C_2T_2\text{-avg}}$). We also found that within each group, binding energies tended to become more stable as the valence shell of the metal increased (*e.g.*, $E_{\text{B-Ti}_3C_2T_2\text{-avg}} > E_{\text{B-Zr}_3C_2T_2\text{-avg}} > E_{\text{B-Hf}_3C_2T_2\text{-avg}}$). Notably, MXenes with molecular terminations, –NH and –OH, typically had weaker binding energies than the atomic terminations. Since the –F and –O terminations are so stable, terminating MXenes with other species may require non-aqueous synthesis methods, such as using molten inorganic salts.[48–51] Indeed, all the considered terminations have been successfully incorporated into MXenes,[49,51,112] albeit thus far only with a few select metals (*e.g.*, Ti, Nb, Ta).

3.1.3 Lattice constants. We report, in Fig. 6 and Table S4, calculated lattice constants for bare MXenes. The lattice constant values for bare MXene structures ranged from 2.87 Å (Mo_3C_2 and W_3C_2) to 3.35 Å (Zr_3C_2), with an average value of 3.08 Å. We found that, with the exception of V_3C_2, the lattice constants of bare MXenes decreased as the number of valence d electrons increased across a given period (*e.g.*, $a_{Zr_3C_2} > a_{Nb_3C_2} > a_{Mo_3C_2}$). This trend was also found in previous studies of M_3C_2,[60,80] and in a study of M_2XS_2.[73] Yang *et al.* attributed the decreased lattice constant to a decrease in length of metal bonds as the number of valence d electrons increased.[73] Notably, atomic radii decreases as the number of d electrons increases within a period, and this trend follows the same pattern in our lattice constants. In fact, we found a strong correlation (+0.83) between our predicted lattice constant for bare MXenes and the atomic radii of the metal atoms. The same study by Yang *et al.*[73] further noted that the lattice constants for those MXenes with 4d transition metals are larger than for those with 3d transition metals, due to an increase in ionic radius. They found that the lattice constants of MXenes

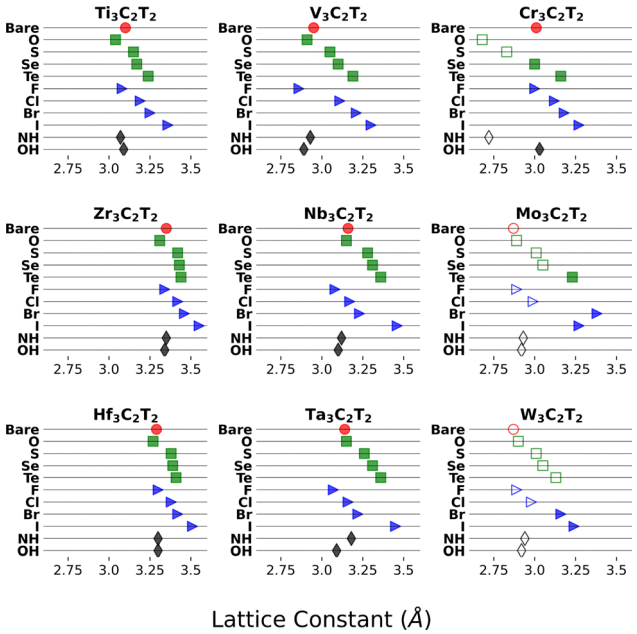

Fig. 6 Lattice constants (Å) for MXenes in their most stable configurations. Red circles are bare structures, green squares have terminations from chalcogens, blue triangles have terminations from halogens, while black diamonds are –OH and –NH terminations. Hollow markers indicate an ABA configuration, while solid markers indicate an ABC configuration.

with 4d transition metals were also larger than those with 5d transition metals, which was attributed to a reduction in metal bond lengths due to scalar-relativistic effects. We also observed that the calculated lattice constant values for bare M_3C_2 MXenes were largest for structures with 4d transition metals, as compared to the lattice constants of the 3d and 5d transition metals in the same group (*e.g.*, $a_{Zr_3C_2} > a_{Hf_3C_2} > a_{Ti_3C_2}$).

The calculated lattice constant values for all configurations of the terminated MXenes are found in Table S5. Our discussion, however, is limited to the lattice constant values for the most stable configurations of the terminated MXenes, which are shown in Fig. 6. These lattice constant values ranged from 2.68 Å ($Cr_3C_2O_2$) to 3.55 Å ($Zr_3C_2I_2$), with an average lattice constant value of 3.17 Å. We expect the size of the terminated MXenes to be influenced by both the metal and termination. Especially when the size of both the termination and metal are larger, it is expected to lead to larger lattice constants. Indeed, our data showed that the lattice constant of atomic-terminated MXenes were moderately correlated with the atomic radii of both metal and termination atoms, with correlation coefficients of, respectively, +0.65 and +0.56.

In most cases, chalcogen terminations resulted in smaller lattice constants compared to the halogen terminations with the same valence shell (*e.g.*, $a_{M_3C_2S_2\text{-Avg}} < a_{M_3C_2Cl_2\text{-Avg}}$). This corresponded with our finding in Section 3.1.2 that chalcogen terminations tended to result in stronger binding energies compared to the halogen terminations with the same valence shell. Other work[60,67] has also reported larger lattice constants for halogen terminations compared to their corresponding chalcogen terminations. Additionally, we noted that the average lattice constant of terminated structures decreased as the number of valence d electrons of the metal increased (*e.g.*, $a_{Zr_3C_2T_2\text{-avg}} > a_{Nb_3C_2T_2\text{-avg}} > a_{Mo_3C_2T_2\text{-avg}}$), which was also found to be the case for bare MXenes. Those MXenes with –NH and –OH terminations have lattice constants similar to those with –O and –F, respectively, likely due to electronic similarities.[31,60,113,114]

For these MXenes that show a preference for ABA stacking, our calculated ABA lattice parameter values were 0.7–5.9% smaller than our calculated values for the corresponding termination site with ABC stacking (see Table S5). This is in agreement with previous studies which found that ABA stacking leads to lattice parameters which are reduced by up to 8% compared to ABC stacking.[34,66,80] This reduction was attributed to reduced steric and/or coulombic repulsion between metal atoms in ABA stacking compared to ABC stacking.[34]

3.2 Electronic properties

3.2.1 Atomic charges. Atomic charges provide insight on electron transfer between the components of the MXenes, including the nature of bonding between atoms, and the oxidation state of the individual elements. We report Bader charges of the different atoms in Tables S7–S9. Fig. S6 also provides the charges of surface metal atoms and the terminations for the most stable MXenes.

Unsurprisingly, all metals were positive (cationic) in the MXenes, while the terminations were negative (anionic). The charges of surface layer metal atoms in bare MXenes ranged from 0.60 (Mo_3C_2) to 1.20 (Hf_3C_2), with an average value of 0.97. On the other hand, surface metals for terminated MXenes ranged from 0.94 ($W_3C_2Te_2$) to 2.23 ($Zr_3C_2O_2$), with an average value of 1.56. The terminations thus induce the metals to become more oxidized. Termination charges on the other hand had smaller absolute values, and ranged from −1.26 ($Zr_3C_2I_2$) to −0.16 ($W_3C_2O_2$), with an average value of −0.67. Average charges of –NH ($Q_{T\text{-}M_3C_2(NH)_2\text{-Avg}} = -0.98$) and –OH ($Q_{T\text{-}M_3C_2(OH)_2\text{-Avg}} = -0.75$) were comparable to, respectively, –O and –F terminations ($Q_{T\text{-}M_3C_2O_2\text{-Avg}} = -1.08$, $Q_{T\text{-}M_3C_2F_2\text{-Avg}} = -0.73$). This observation may be explained by electronic similarities between the respective atomic (–O/–F) and molecular terminations (–NH/–OH).[31,60,113,114] Our data showed that more stable terminations were more anionic. We found a correlation coefficient of +0.85 between termination Bader charge and termination binding energy for the atomic species, confirming the relationship between charge and stability. Thus, we conclude that more oxidation/reduction results when stronger interactions occur between the metal and termination.

Furthermore, we found a relationship between Bader charge values and atomic electronegativity. Our predicted decrease in metal charges corresponded to increased electronegativity of the metal atom. For bare MXenes, there was a correlation coefficient of −0.90 between the Bader charges of surface metal atoms and electronegativity of the metal species. For terminated MXenes, the correlation coefficient was −0.69. Thus, metal atoms with larger electronegativity are less likely to be oxidized since they tend to attract electrons. In contrast, the

termination charges became more negative with increased electronegativity of the termination atom, since atoms with larger electronegativity will attract more electrons and become more negative. The correlation coefficient between termination electronegativity and termination Bader charge was −0.60.

3.2.2 Work function. All work function values are reported in Fig. 7 and Table S10. The work function for the bare structures ranged from 4.11 eV (Zr_3C_2) to 4.92 eV (W_3C_2), with an average value of 4.53 eV. This was a very narrow range despite the variety of metals in the MXenes, indicating that it may be difficult to tune the work function of bare MXenes. On the other hand, terminated MXenes had a much wider range, from 1.67 eV ($Cr_3C_2(OH)_2$) to 7.80 eV ($Cr_3C_2O_2$). Generally halogen terminations had lower work functions than chalcogen terminations, as the average work function for halogen terminated MXenes (4.27 eV) was found to be nearly 1 eV lower than the average work function of chalcogen terminated MXenes (5.25 eV). Particularly, –O terminations resulted in the largest work functions for all MXenes with group 5 and 6 metals ($\phi_{M_3C_2O_2\text{-avg}}$ being 5.75 and 7.46 eV with, respectively, group 5 and 6 metals), while –S terminations produced the largest work functions for those with group 4 metals ($\phi_{M_3C_2S_2\text{-avg}}$ was 6.33 eV with group 4 metals). On the other hand, –Te and –I terminated MXenes resulted in the lowest average work functions ($\phi_{M_3C_2Te_2\text{-avg}}$ = 4.09 eV, $\phi_{M_3C_2I_2\text{-avg}}$ = 3.61 eV) for atomic terminations.

Work functions for MXenes terminated by OH groups, however, ranged from 1.67 eV ($Cr_3C_2(OH)_2$) to 3.05 eV ($W_3C_2(OH)_2$), with an average value of 2.34 eV. These results for –OH agree with literature, where it has been well established that –OH terminated MXenes display ultralow work functions.[38–40,60,65] The work function values of –NH terminated MXenes ranged from 2.28 eV ($Ta_3C_2(NH)_2$) to 3.31 eV ($Nb_3C_2(NH)_2$), and had an average value of 2.82 eV, again being ultralow work functions. Thus, termination selection is crucial for engineering MXene work function while choice of metal may be less important.

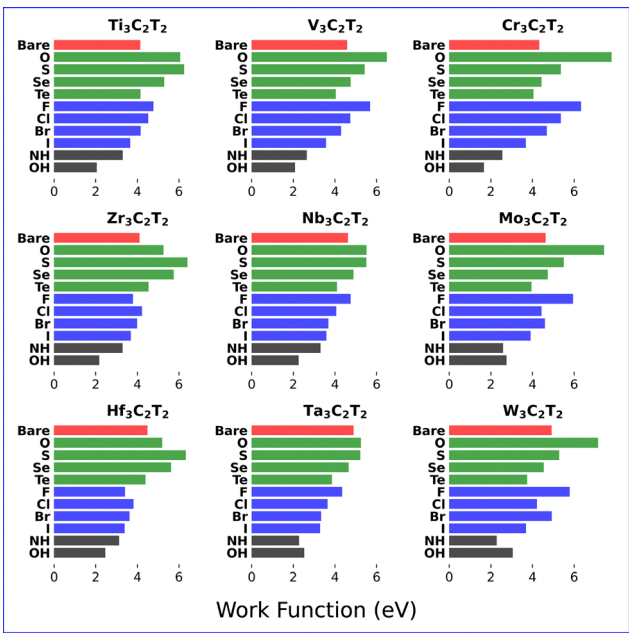

Fig. 7 Work functions (eV) for MXenes in their most stable configurations. Red lines are bare MXenes, green lines are chalcogen terminated, blue lines are halogen terminated, and black lines are OH and NH terminated.

Because the work function is such a critical electronic property, there have been a number of attempts to explain the work functions of materials, including dependence on various material properties.[34,38,39,42,65,67,68,115–121] Although these studies report connections between work function and various properties, quantitative analysis connecting these properties to the work function is generally lacking. Thus, we calculated the correlation coefficients between the MXene work function and various atomic properties, as well as between the work function and other MXene properties (see Table S11). Atomic properties of the metal and terminating atoms were taken from the Mendeleev database.[103] MXene properties (*e.g.*, termination binding energy, M–T bond distances, Bader charges, p-band center) were from our calculations, and are reported in various tables in the SI.

The highest correlations occurred with termination atomic volume (−0.74), termination p-band center (+0.70), termination specific heat capacity (+0.67), M–T bond distance (−0.66), termination Mendeleev number (−0.65), termination atomic number (−0.64), termination atomic weight (−0.63), termination double covalent radius (−0.63), termination period number (−0.63), and termination triple covalent radius (−0.61). These correlations indicate that the termination, rather than the metal, is key to the MXene work functions. It is worth noting that a number of these properties, namely atomic volume, specific heat capacity, M–T bond distance, atomic weight, period number, and covalent radii, are all interrelated. In particular, we found that each of these properties were highly correlated with the atomic number of the corresponding termination atom (correlation coefficients being $\geq |0.78|$).

3.2.3 Conducting nature. We calculated the density of states and band gaps to establish the conducting nature of the MXenes (*e.g.*, semiconducting or metallic). The PBE functional is widely utilized for many calculations, but is well known to underestimate band gaps,[122–124] so we also calculated the DOS and band gap values using the HSE06 functional. We must acknowledge that the HSE06 functional may not be accurate for describing properties of metals[125–127] and, in some cases, has been found to overestimate the band gap.[122,123,127–129]

Our results for MXene electronic structure using the PBE functional indicated that all 99 $M_3C_2/M_3C_2T_2$ MXenes were metallic. DOS plots calculated using the PBE functional can be found in Fig. S11–S19. When using the HSE06 functional, however, we predicted 21 MXenes to be narrow-gap semiconductors. Band gap values (calculated with HSE06) are given in Table 1, and the corresponding DOS plots are given in Fig. S8–S10. In accordance with the definition of semiconductors presented by Sheng S. Li,[130] we considered only those with $E_g > 0.1$ eV to be semiconducting. These MXenes included three Ti-based MXenes, Cr_3C_2, $Zr_3C_2(NH)_2$, six Nb-based MXenes, Mo_3C_2, two Hf-based MXenes, three Ta-based MXenes, and four W-based MXenes. Every

Table 1 Band gap values (E_g) for MXenes which were identified as semiconductors using the HSE06 functional. Band gap values are given in units of eV. Corresponding DOS plots for each semiconducting MXene are given in Fig. S8–S10

MXene	E_g	MXene	E_g
$Ti_3C_2O_2$	0.14	Mo_3C_2	0.23
$Ti_3C_2I_2$	0.15	$Hf_3C_2O_2$	0.18
$Ti_3C_2(NH)_2$	0.15	$Hf_3C_2(NH)_2$	0.30
Cr_3C_2	0.48	$Ta_3C_2Se_2$	0.24
$Zr_3C_2(NH)_2$	0.26	$Ta_3C_2Cl_2$	0.54
$Nb_3C_2S_2$	0.24	$Ta_3C_2Br_2$	0.47
$Nb_3C_2Se_2$	0.18	W_3C_2	0.20
$Nb_3C_2F_2$	0.65	$W_3C_2O_2$	0.32
$Nb_3C_2Cl_2$	0.51	$W_3C_2S_2$	0.19
$Nb_3C_2Br_2$	0.47	$W_3C_2(NH)_2$	0.25
$Nb_3C_2(OH)_2$	0.12		

termination, except Te, when combined with the right metal, formed a semiconductor MXene. The band gap values for these structures ranged from 0.12 eV ($Nb_3C_2(OH)_2$) to 0.65 eV ($Nb_3C_2F_2$). Literature has largely focused on predicting band gaps for M_2CT_x MXenes,[33,42,131–136] leaving questions about $M_3C_2T_x$ MXenes. Indeed, we are not aware of previous electronic structure calculations using the HSE06 functional for most MXenes we predicted ($n = 2$ MXenes) to be semiconducting. In the case of MXenes which have previous electronic structure calculations using the HSE06 functional, there is disagreement throughout literature. $Hf_3C_2O_2$ has been found to be a semiconductor with reported band gaps of 0.16 eV,[137] (similar to our value of 0.18 eV), 0.43 eV,[138] and 0.95 eV.[139] We report a band gap of 0.14 eV for $Ti_3C_2O_2$, while other papers[140] found it to be metallic. Literature also predicts M_2CO_2 (M = Hf, Zr, Ti) MXenes to be semiconductors,[33] while we also predict several O-terminated MXenes to be semiconductors.

Despite DFT predictions of semiconductors, experimental studies identifying semiconductor MXenes are limited.[132,141,142] The discrepancy between theoretical predictions and experimental results regarding electronic properties of MXenes has been attributed to defects[143] and mixed terminations[132] which may be introduced during synthesis. Thus, overcoming current synthesis challenges may be the key to experimental realization of semiconducting MXenes. Our work may further provide direction on what compositions may be worth pursuing to create semiconductor MXenes.

Electrical conductivity is another important property of MXenes, especially for applications such as catalysis, spintronics, batteries, LEDs, photodetectors, and others. However, calculating electrical conductivity can be difficult since it depends on many factors, such as charge carrier concentration (which in turn depends on donor state concentration) and charge mobility. Rather, we examined the DOS values at the Fermi level, $N(E_F)$, which has been used as a proxy for electrical conductivity in metal MXenes.[140,144–147] Larger DOS at the E_F should in principle correspond to larger carrier concentration since more free electrons would be available. We report, in Fig. S7 and Table S12, $N(E_F)$ values as calculated with the PBE functional. We do not report $N(E_F)$ values using the HSE06 functional, since this functional may have low accuracy for predicting properties of metals.[125–127] The $N(E_F)$ values spanned 0.49 states per eV ($Hf_3C_2O_2$) to 6.08 states per eV ($Cr_3C_2Te_2$). The metals Ti, Zr, and Hf had some of the lowest values of $N(E_F)$, indicating potentially low electrical conductivity for these MXenes. This is noteworthy, considering that M_2CO_2 with M = Ti, Zr, and Hf are the MXenes most frequently predicted to be semiconducting.[31,33–35,58,59,148] The highest values of $N(E_F)$ were found to be with Cr- and V-based MXenes, having average $N(E_F)$ values of 1.33 and 1.22 states per eV respectively, compared to an overall average value for all MXenes of 0.87 states per eV. This suggests that such MXenes may have larger electrical conductivity.

The termination had an important impact on the $N(E_F)$ values, with strong interplay between the metal and termination. For example, we calculated a correlation coefficient between the electron count (which depends on the metal and termination; see Section 3.1.1) and $N(E_F)$ values to be +0.46, indicating at least a modest correlation between the two. Furthermore, we found that $N(E_F)$ values of terminated MXenes were correlated more strongly (−0.64) with the atomic volume ratio, $V_{M/T}$, than with any elemental properties of the metal or termination atom alone. For MXenes terminated by chalcogens, at least for groups 4 and 6, the $N(E_F)$ values tended to increase with increasing atomic number of the chalcogen termination. Particularly, –Te terminations resulted in some of the MXenes with the highest $N(E_F)$ values. On the other hand, group 5 metals showed the opposite trend where $N(E_F)$ values tended to decrease with increasing atomic number of the chalcogen termination. Halogen terminations gave low $N(E_F)$ values with group 4 metals, larger $N(E_F)$ values with group 5 metals that tended to increase with termination atomic number, and high $N(E_F)$ values with group 6 metals. The –OH and –NH terminations yielded moderate $N(E_F)$ values with group 4 metals, relatively high values with group 5 metals, and both low (NH) and high (OH) $N(E_F)$ values with group 6 metals. Interestingly, we found that the lowest values of $N(E_F)$ for MXenes with group 6 metals were those with the ABA-hX configuration (*i.e.*, $Cr_3C_2T_2$ with T = O, S, and NH, $Mo_3C_2T_2$ with T = O, S, Se, and NH, and $W_3C_2T_2$ with T = O, S, Se, Te and OH). Thus, our results show that there are strong interactions between the metal and termination that may affect the conductivity, and these interactions are complex.

3.2.4 d-band center. The d-band center (ε_d) of a metal has been established as a good descriptor for predicting adsorption energies and surface reactivity.[97,98,149] The d-band center of MXenes has been linked to their performance as supercapacitors,[150] gas sensors,[151] and catalysts.[152–154] We report, in Fig. 8 and Table S13, the d-band center of the MXenes in their most stable configurations. The d-band centers of bare MXenes decreased (*i.e.*, shifted further from E_F) as the number of valence d electrons increased (*e.g.*, $\varepsilon_{d\text{-}Ti_3C_2} > \varepsilon_{d\text{-}V_3C_2} > \varepsilon_{d\text{-}Cr_3C_2}$), similar to what was reported by Hammer and Nørskov.[149] A similar trend is that d-band centers become more negative with larger valence shells (*e.g.*, $\varepsilon_{d\text{-}Ti_3C_2} > \varepsilon_{d\text{-}Zr_3C_2} > \varepsilon_{d\text{-}Hf_3C_2}$).

Our calculated values of the d-band center for terminated MXenes ranged from −3.49 eV ($W_3C_2O_2$) to −0.61 eV ($Ti_3C_2I_2$). The d-band center trends of terminated MXenes were similar to

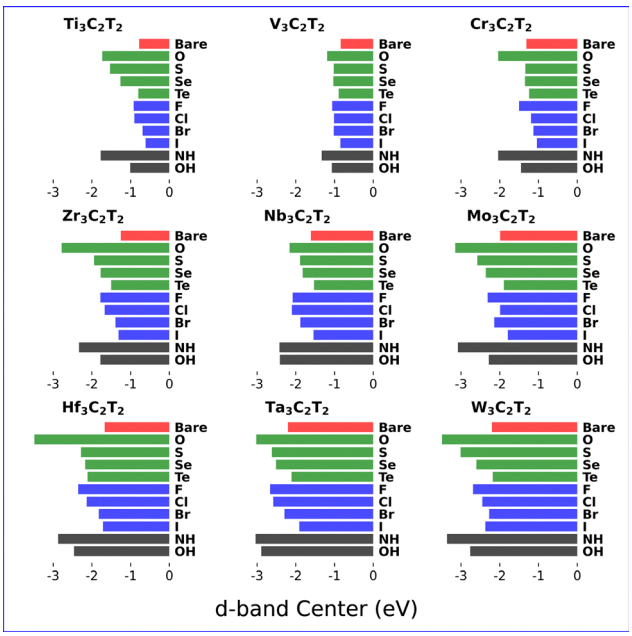

Fig. 8 Calculated d-band center values (eV) of MXenes in their most stable configurations. Energies are relative to the Fermi energy (0 eV). Results are using the PBE functional. Red lines are bare MXenes, green lines are chalcogen terminated, blue lines are halogen terminated, and black lines are OH and NH terminated.

the trends of bare MXenes. Regardless of termination species, the d-band center of $M_3C_2T_2$ MXenes decreased as the metal valence shell increased (*e.g.*, $\varepsilon_{\text{d-Ti}_3\text{C}_2\text{T}_2} > \varepsilon_{\text{d-Zr}_3\text{C}_2\text{T}_2} > \varepsilon_{\text{d-Hf}_3\text{C}_2\text{T}_2}$). In general, the d-band center of terminated MXenes also decreased as the number of metal valence d electrons increased (*e.g.*, $\varepsilon_{\text{d-Zr}_3\text{C}_2\text{T}_2\text{-Avg}} > \varepsilon_{\text{d-Nb}_3\text{C}_2\text{T}_2\text{-Avg}} > \varepsilon_{\text{d-Mo}_3\text{C}_2\text{T}_2\text{-Avg}}$).

Indeed, we found a correlation of −0.78 between metal atomic number and our calculated values of metal d-band centers for terminated MXenes, indicating the strong dependence of the d-band center on the metal choice. In addition to the strong effect of the metal on d-band center, the termination also affected the d-band center significantly. For example, $Hf_3C_2O_2$ had a d-band center of −3.48 eV, while $Hf_3C_2I_2$ had a d-band center of −1.71 eV, a difference of 1.77 eV. Generally chalcogen-terminated MXenes had more negative d-band centers compared to halogen-terminated MXenes within the same row of the periodic table. We also found that –NH/–O and –OH/–F terminations resulted in similar values of ε_d, each pair having electronic similarities.[31,60,113,114]

3.3 Mechanical properties

Materials with desirable mechanical properties are key for many applications, such as biomedical devices, strain sensors, flexible electronics, microfluidic devices, and composite materials. We calculated 2D mechanical properties, including elastic constants (C_{11} and C_{12}), Young's modulus (E), Poisson's ratio (ν), shear modulus (G), and bulk modulus (K). Calculated mechanical properties are reported in Table S15. All MXenes were found to be mechanically stable according to the elastic stability criteria ($C_{11} > 0$ and $C_{11} > |C_{12}|$).[96,155]

Young's modulus functions as a measure of material limitations, influencing the operating conditions which will result in deformation, as well as typifying material stiffness. It should be noted that we found the elastic constant C_{11}, shear modulus, and bulk modulus (Table S15) to be highly correlated to Youngs modulus (correlation coefficient ≥ 0.90). Elastic constant C_{12} and Poisson's ratio were also correlated with each other (0.74). We therefore focused our discussion on Youngs modulus and Poisson's ratio, since these two are representative mechanical properties.

3.3.1 Young's modulus. We show in Fig. 9 and Table S15 calculated Young's modulus values. We found that Young's modulus values ranged from 93 N m^{-1} ($Ti_3C_2Te_2$) to 535 N m^{-1} ($W_3C_2O_2$), with an average value of 308 N m^{-1}. For a given valence shell, we found that average Young's modulus values were larger for chalcogen terminated MXenes as compared to those with the corresponding halogen terminations (*e.g.*, $E_{\text{M}_3\text{C}_2\text{O}_2\text{-avg}} > E_{\text{M}_3\text{C}_2\text{F}_2\text{-avg}}$). Also, MXenes with chalcogen terminations typically showed greater variability in Young's modulus values compared to those with halogen terminations. The range of Young's modulus values for chalcogen-terminated MXenes was 442 N m^{-1}, with a standard deviation of 113 N m^{-1}, while the range for halogen-terminated MXenes was 364 N m^{-1} with a standard deviation of 89 N m^{-1}.

MXenes with –O and –F terminations produced the highest values of Youngs modulus for atomic-terminated structures, with average values of 414 N m^{-1} and 339 N m^{-1}, respectively. In comparison, the 2D Young's modulus for graphene is around 340 N m^{-1}.[67,156] MXenes with –NH terminations also had large Young's modulus values, having an average of 400 N m^{-1}. These

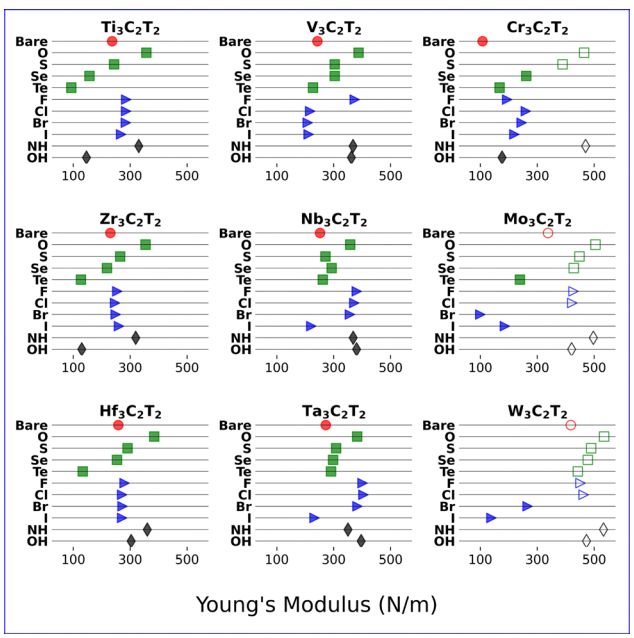

Fig. 9 Young's modulus (N m^{-1}) for MXenes in their most stable configurations. Red circles are bare structures, green squares have terminations from chalcogens, blue triangles have terminations from halogens, while black diamonds are –OH and –NH terminations. Hollow markers indicate an ABA configuration, while solid markers indicate an ABC configuration.

results can be explained, at least in part, by considering our calculated Bader charges in Section 3.2.1 (Fig. S6 and Tables S7, S8), which showed that –O and –NH terminations resulted in the highest M–T charge transfer (*i.e.*, large positive charges on the metal and large negative charges on the termination). Increased charge transfer corresponds to stronger bonds and, therefore, to stiffer materials. This is also corroborated by the large binding energies of –O.

We also considered the impact of the metal on MXene stiffness. On average, Zr-based MXenes had the lowest values of Young's modulus ($E_{Zr_3C_2T_2\text{-avg}} = 241$ N m^{-1}), while W-based MXenes had the highest values ($E_{W_3C_2T_2\text{-avg}} = 426$ N m^{-1}). Our results showed that metals with more valence d electrons tended to have larger Youngs modulus values (*e.g.*, $E_{Zr_3C_2T_2\text{-avg}} < E_{Nb_3C_2T_2\text{-avg}} < E_{Mo_3C_2T2\text{-avg}}$). Within a given metal group, Youngs modulus values tended to increase as the valence shell increased (*e.g.*, $E_{V_3C_2T_2\text{-avg}} < E_{Nb_3C_2T_2\text{-avg}} < E_{Ta_3C_2T_2\text{-avg}}$).

It is well known that Youngs modulus is affected by the crystal structure, and MXenes are no exception. Our results showed that ABA stacking resulted in larger Young's modulus values compared to ABC stacking. We found that Youngs modulus for MXenes with ABC stacking ranged from 93 N m^{-1} ($Ti_3C_2Te_2$) to 404 N m^{-1} ($Ta_3C_2Cl_2$), with an average value of 271 N m^{-1}, while the Youngs modulus for MXenes with ABA stacking (shown with hollow markers in Fig. 9) ranged from 338 N m^{-1} (Mo_3C_2) to 535 N m^{-1} ($W_3C_2O_2$), with an average value of 455 N m^{-1}. A comparison between ABC-hM and ABC-hX indicated the ABC-hX configuration resulted in some of the highest values of Youngs modulus. For those MXenes which preferred the ABC-hX configuration (*e.g.*, $M_3C_2T_2$ with M = V, Nb, Ta and T = F, OH) Young's modulus values ranged from 357 N m^{-1} ($Nb_3C_2Br_2$) to 404 N m^{-1} ($Ta_3C_2Cl_2$), with an average value of 380 N m^{-1}. Kazemi *et al.* also reported larger Youngs modulus values for ABC-hX configurations compared to ABC-hM.[68]

3.3.2 Poisson's ratio. Poisson's ratio (ν) is an indicator of material flexibility. Specifically, it is a measure of the deformation perpendicular to an applied force. We found the Poisson's ratio values, reported in Table S15, to have a range from −0.40 ($W_3C_2I_2$) to 0.75 ($Ti_3C_2Te_2$), with an average value of 0.26. A box plot of the values for bare and terminated MXenes is shown in Fig. S20. In fact, although the range of values was 1.15, the standard deviation was only 0.15, indicating most values were close to the average of 0.26. Indeed, the 25th percentile was 0.20, while the 75th percentile was 0.29. Fig. S20 shows the distribution of values, and indicates that, other than a few outliers, there is very little variation in our data, regardless of metal or termination. Some MXenes are rather unique, and are discussed in the following paragraph.

We found eight MXenes with Poisson's ratio values >0.5, which is typically indicative of instability under stress.[157,158] These included $M_3C_2Te_2$ with M = Ti, Zr, Hf, and Cr, and $M_3C_2(OH)_2$ with M = Ti, and Zr. On the other extreme, we found three MXenes with a negative Poisson's ratio (NPR). This occurs when a material expands, rather than contracts, perpendicular to applied strain (*i.e.*, it becomes wider when stretched). This phenomena is rare, but has been predicted for a number of 2D materials.[159–163] We found NPR values for Cr_3C_2 (−0.15), $W_3C_2Br_2$ (−0.02), and $W_3C_2I_2$ (−0.40). These materials are therefore expected to exhibit enhanced toughness and vibrational damping compared to a MXene with a positive Poisson's ratio.[162,163] Our results are corroborated by experimental studies which reported NPR values for some MXenes with group 6 metals.[159,160] For example, Wu *et al.*[159] reported a NPR of −0.43 for W_2C and Mortazavi *et al.*[160] reported an NPR of −0.15 for Mo_2C.

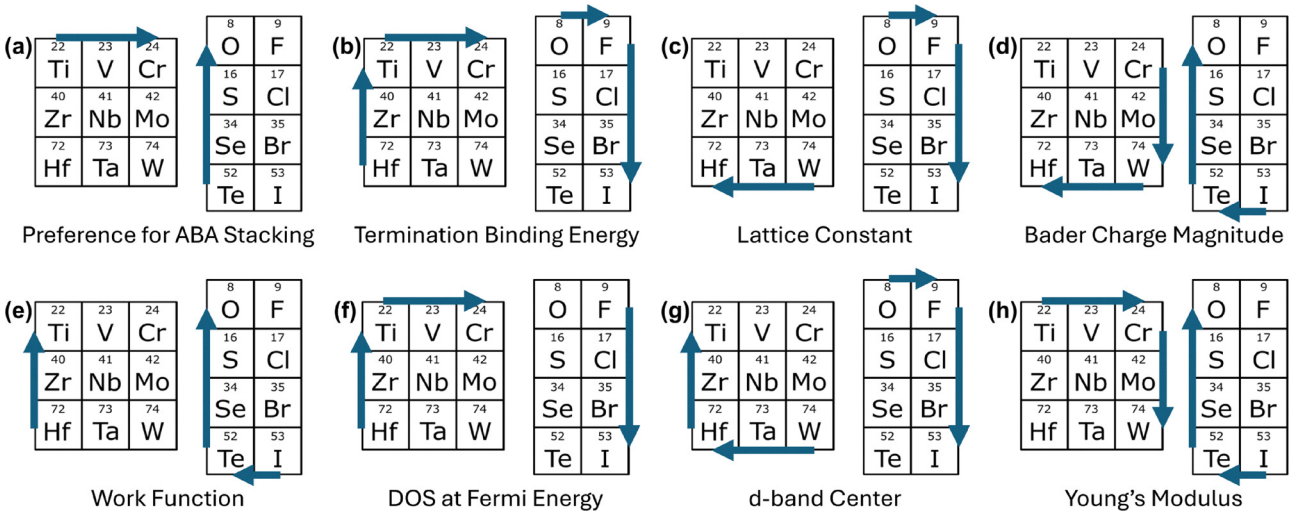

Fig. 10 A summary of our findings regarding the general impact of metal and termination species on the preference for ABA stacking (a), termination binding energy (b), lattice constant (c), the magnitude of Bader charges for termination and surface layer metal atoms (d), work function (e), DOS at Fermi energy (f), metal d-band center (g), and Young's modulus (h). Arrows point in the direction of generally increasing values. Arrows are only shown for discernible trends, as a clear relationship was not always present (*e.g.*, lattice constant and metal period). Poisson's ratio is not shown, as we found no distinct trends in the data.

3.4 Summarizing the composition–property relationships

Throughout this work, we calculated various structural, electronic, and mechanical properties of $M_3C_2/M_3C_2T_2$ MXenes. Identifying how these properties are influenced by metal choice and termination species is important for optimizing MXenes for targeted applications. In Fig. 10, we summarize the trends in how the various properties depend on the group and period of the metals and terminations. For each property, arrows point in the direction of increasing values. For example, it can be seen that termination binding energies, lattice constants, and d-band centers all increase by selecting a halogen termination, rather than a chalcogen termination. On the other hand, work function and Young's modulus values would tend to increase for chalcogens compared to halogens. Similar relationships are shown for how termination period affects different properties (*e.g.*, termination binding energy increases with increased period or atomic number). Fig. 10 also shows how metal period and group affects the various calculated properties. Our work indicates which metal and termination choices should be selected to obtain desired properties.

3.5 Notable MXenes

In addition to identifying the general relationships between MXene properties and their composition, we also identified some promising MXenes for various applications. For example, when combined with –O terminations, group 6 metals resulted in $\phi > 7$ eV ($\phi_{Cr_3C_2O_2}$ = 7.80 eV, $\phi_{Mo_3C_2O_2}$ = 7.44 eV, $\phi_{W_3C_2O_2}$ = 7.15 eV), which are considered ultra-high work functions.[164] Ultra-high work functions may be desirable for applications involving electron capture and storage, such as in LEDs,[165–167] transistors,[168–170] and electron capture in solar cells.[171–173] Several MXenes were identified as having low work functions (<3 eV), predominantly those terminated with NH or OH groups. These include all the metals (except W) with –OH terminations. These also include M = V, Cr, Mo, Ta, and W with –NH terminations. MXenes with ultra-low values may be ideal for facilitating charge transport in applications including electron emission devices,[174–176] hydrogen production,[177–179] and thermionic energy conversion.[65,180,181]

Furthermore, we identified several potential semiconductors, as presented in Table 1. These MXenes may be useful in electronic, photocatalysis, sensor, and thermoelectric applications.[32,182,183] As discussed in Section 3.2.3, several MXenes were identified as having low conductivity (*e.g.*, $Ti_3C_2O_2$, $Zr_3C_2O_2$, and $Hf_3C_2O_2$), while other MXenes were identified as having high conductivity (*e.g.*, $Cr_3C_2Te_2$ and $Mo_3C_2Br_2$). High conductivity may be desirable for energy storage, sensing applications, electronic devices, thermoelectrics, and other applications.[22,183] Finally, we note that higher d-band center values may lead to better catalytic reactivity,[154] increased capacitance in supercapacitors,[150] or improved gas sensing ability.[151] Metals with heavier halogens (such as I and Br) tended to have the highest d-band centers, especially when paired with Ti, V, or Cr.

Identifying MXenes with desirable mechanical properties may also be important. High stiffness for –O terminated MXenes, as compared to other terminations, has been widely reported in literature.[35,67,68,70,78,184] In addition to –O, we found that –NH terminated MXenes also exhibited superior stiffness compared to other terminations, with an average Youngs modulus value of 400 N m^{-1}. The highest Young's modulus values occurred with Mo- and W-based MXenes (*e.g.*, 535 N m^{-1} for $W_3C_2O_2$, 533 N m^{-1} for $W_3C_2(NH)_2$, and 505 N m^{-1} for $Mo_3C_2O_2$), which incidentally preferred ABA stacking. These MXenes may be useful for applications where high stiffness is desired, such as in protective coatings,[185–187] biomedical applications,[188–190] or composite materials.[191–193] On the other hand, some MXenes had low Young's modulus values ($\approx$100 N m^{-1}), such as $Ti_3C_2Te_2$, Cr_3C_2, and $Mo_3C_2Br_2$. Due to our predicted combination of low Young's modulus and high electrical conductivity for those three MXenes, they may be of particular interest in flexible, wearable sensors.[194–196]

We noted in Section 3.3.2 that most MXenes had Poisson's ratio values near 0.26. Several MXenes ($M_3C_2Te_2$ with M = Ti, Zr, Hf, and Cr, and $M_3C_2(OH)_2$ with M = Ti, and Zr) had high values (>0.5), indicating their instability under stress. A few MXenes (Cr_3C_2, $W_3C_2Br_2$, $W_3C_2I_2$) had negative Poisson's ratios, which may make them potentially suitable for use in sensors, biomedical devices, clothing, and other applications.[162,197]

As noted here and in Sections 3.2 and 3.3, several MXenes with non-traditional terminations (–O, –OH, –F) have interesting properties. For instance, –Te and –I terminated MXenes have a unique combination of properties, including large lattice constants (*i.e.*, large surface to volume ratio), low work function, high electrical conductivity, high d-band center values, and low Young's modulus, which make them strong candidates for a variety of applications. However, these terminations have the lowest binding energies. Therefore, the continued development of synthesis methods which overcome thermodynamics issues, and produce MXenes with heavy terminations may be beneficial to the field. For example, molten salt etching,[49] electrochemical etching,[51] and chemical vapor deposition[198] have all been shown to provide significant control over the resulting termination species and coverage.

4 Conclusions

In this study, we modeled 99 different $M_3C_2/M_3C_2T_2$ MXenes in order investigate the impact of chemical composition on their structural, electronic, and mechanical properties. We considered an extended compositional space compared to most previous MXene studies. This included M = Ti, V, Cr, Zr, Nb, Mo, Hf, Ta, and W with T = bare, O, S, Se, Te, F, Cl, Br, I, NH, and OH. We first predicted the most stable configuration for each MXene (*i.e.*, stacking and termination site), which required over 700 simulations. Our calculations showed that most MXenes had an energetic preference for ABC stacking, but some group 6 metals preferred ABA stacking (20% of the studied MXenes). We found that stacking and termination site preference were related to electron count and metal/termination atomic volume ratio. The MXene lattice constants were found to be highly dependent on the atomic configurations, and was found to be

proportional to metal and termination atom sizes. We also calculated termination binding energies and found that the common –O and –F terminations were significantly more stable than other terminations, presenting a challenge for synthesizing MXenes with other terminations.

We determined a number other properties, including electronic and mechanical properties. Several properties strongly depended on the metal and termination, and the trends for such properties were established (see Fig. 10). We identified several notable MXenes, with interesting calculated properties. For example, MXenes terminated with –NH and –OH generally had ultra low work functions, while $M_3C_2O_2$ MXenes with M = Cr, Mo, W had ultra high work functions. We found the termination had a much greater effect than metal choice on the work function. Using the HSE06 functional, we classified several MXenes as narrow-gap semiconductors (see Table 1). Every termination could form a semiconducting MXene when paired with the right metal, with the exception of –Te. Some MXenes (typically halogen terminations with period 4 metals) had higher d-band centers, which may be useful for catalysis, energy storage, or gas sensing. Our calculations of mechanical properties showed that –O and –NH terminations resulted in very stiff MXenes. ABA stacking also led to stiffer MXenes, compared to ABC stacking. Most Poisson's ratio values were near the average of 0.26, but three MXenes had a negative Poisson's ratio. To summarize, we have shown how termination and metal choices affect various properties of MXenes. We identified the trends of such properties, and our work provides guidance and motivation to synthesize and study MXenes beyond typical MXenes, *e.g.*, beyond $Ti_3C_2O_2$ or $Ti_3C_2F_2$.

Author contributions

ES performed the DFT simulations, analyzed the results, and contributed to the writing of the paper. BT performed DFT simulations. NAD oversaw the project and contributed to the writing.

Conflicts of interest

There are no conflicts to declare.

Data availability

Data from the various tables and figures for this article have been included in the SI. See DOI: **https://doi.org/10.1039/d5ma00874c**

Simulation files, including geometries, can be found at **https://github.com/Deskins-group/Structure-Files/tree/master/MXene-structure-properties**.

Acknowledgements

This research was supported in part by the National Science Foundation under grant NRT-HDR-2021871. This research was performed using computational resources supported by the Academic & Research Computing group at Worcester Polytechnic Institute.

References

1 Y. Gogotsi and B. Anasori, *ACS Nano*, 2019, **13**, 8491–8494.
2 M. Sokol, V. Natu, S. Kota and M. W. Barsoum, *Trends Chem.*, 2019, **1**, 210–223.
3 L. Verger, V. Natu, M. Carey and M. W. Barsoum, *Trends Chem.*, 2019, **1**, 656–669.
4 X. Jiang, A. V. Kuklin, A. Baev, Y. Ge, H. Ågren, H. Zhang and P. N. Prasad, *Phys. Rep.*, 2020, **848**, 1–58.
5 A. VahidMohammadi, J. Rosen and Y. Gogotsi, *Science*, 2021, **372**, eabf1581.
6 B. Anasori, M. R. Lukatskaya and Y. Gogotsi, *Nat. Rev. Mater.*, 2017, **2**, 1–17.
7 S. Sun, C. Liao, A. M. Hafez, H. Zhu and S. Wu, *Chem. Eng. J.*, 2018, **338**, 27–45.
8 J. Pang, R. G. Mendes, A. Bachmatiuk, L. Zhao, H. Q. Ta, T. Gemming, H. Liu, Z. Liu and M. H. Rummeli, *Chem. Soc. Rev.*, 2019, **48**, 72–133.
9 W. Meng, X. Liu, H. Song, Y. Xie, X. Shi, M. Dargusch, Z.-G. Chen, Z. Tang and S. Lu, *Nano Today*, 2021, **40**, 101273.
10 P. Lokhande, A. Pakdel, H. Pathan, D. Kumar, D.-V. N. Vo, A. Al-Gheethi, A. Sharma, S. Goel, P. P. Singh and B.-K. Lee, *Chemosphere*, 2022, **297**, 134225.
11 Q. Tang, Z. Zhou and P. Shen, *J. Am. Chem. Soc.*, 2012, **134**, 16909–16916.
12 P. Kuang, J. Low, B. Cheng, J. Yu and J. Fan, *J. Mater. Sci. Technol.*, 2020, **56**, 18–44.
13 X. Xie and N. Zhang, *Adv. Funct. Mater.*, 2020, **30**, 2002528.
14 Y. Zhao, M. Que, J. Chen and C. Yang, *J. Mater. Chem. C*, 2020, **8**, 16258–16281.
15 J. K. Im, E. J. Sohn, S. Kim, M. Jang, A. Son, K. D. Zoh and Y. Yoon, *Chemosphere*, 2021, **270**, 129478.
16 A. Liu, X. Liang, X. Ren, W. Guan, M. Gao, Y. Yang, Q. Yang, L. Gao, Y. Li and T. Ma, *Adv. Funct. Mater.*, 2020, **30**, 2003437.
17 H. Wang and J.-M. Lee, *J. Mater. Chem. A*, 2020, **8**, 10604–10624.
18 Y. Wang, Y. Nian, A. N. Biswas, W. Li, Y. Han and J. G. Chen, *Adv. Energy Mater.*, 2021, **11**, 2002967.
19 Z. Kang, M. A. Khan, Y. Gong, R. Javed, Y. Xu, D. Ye, H. Zhao and J. Zhang, *J. Mater. Chem. A*, 2021, **9**, 6089–6108.
20 L.-N. Shi, L.-T. Cui, Y.-R. Ji, Y. Xie, Y.-R. Zhu and T.-F. Yi, *Coord. Chem. Rev.*, 2022, **469**, 214668.
21 H. Kim, Z. Wang and H. N. Alshareef, *Nano Energy*, 2019, **60**, 179–197.
22 F. Shahzad, A. Iqbal, H. Kim and C. M. Koo, *Adv. Mater.*, 2020, **32**, 2002159.
23 A. Ahmed, S. Sharma, B. Adak, M. M. Hossain, A. M. LaChance, S. Mukhopadhyay and L. Sun, *InfoMat*, 2022, **4**, e12295.

24 A. Sinha, Dhanjai, H. Zhao, Y. Huang, X. Lu, J. Chen and R. Jain, *TrAC, Trends Anal. Chem.*, 2018, **105**, 424–435.
25 K. Deshmukh, T. Kovářík and S. P. Khadheer, *Coord. Chem. Rev.*, 2020, **424**, 213514.
26 D. H. Ho, Y. Y. Choi, S. B. Jo, J.-M. Myoung and J. H. Cho, *Adv. Mater.*, 2021, **33**, 2005846.
27 Y. Pei, X. Zhang, Z. Hui, J. Zhou, X. Huang, G. Sun and W. Huang, *ACS Nano*, 2021, **15**, 3996–4017.
28 Y. Gogotsi and Q. Huang, *ACS Nano*, 2021, **15**, 5775–5780.
29 M. Mozafari and M. Soroush, *Mater. Adv.*, 2021, **2**, 7277–7307.
30 T. Su, X. Ma, J. Tong, H. Ji, Z. Qin and Z. Wu, *J. Mater. Chem. A*, 2022, **10**, 10265–10296.
31 M. Khazaei, M. Arai, T. Sasaki, C. Y. Chung, N. S. Venkataramanan, M. Estili, Y. Sakka and Y. Kawazoe, *Adv. Funct. Mater.*, 2013, **23**, 2185–2192.
32 X.-H. Zha, Q. Huang, J. He, H. He, J. Zhai, J. S. Francisco and S. Du, *Sci. Rep.*, 2016, **6**, 27971.
33 Y. Zhang, W. Xia, Y. Wu and P. Zhang, *Nanoscale*, 2019, **11**, 3993–4000.
34 D. Ontiveros, F. Viñes and C. Sousa, *J. Mater. Chem. A*, 2023, **11**, 13754.
35 X. H. Zha, K. Luo, Q. Li, Q. Huang, J. He, X. Wen and S. Du, *EPL*, 2015, **111**, 26007.
36 Z. Guo, J. Zhou, C. Si and Z. Sun, *Phys. Chem. Chem. Phys.*, 2015, **17**, 15348–15354.
37 Y. Bai, K. Zhou, N. Srikanth, J. H. Pang, X. He and R. Wang, *RSC Adv.*, 2016, **6**, 35731–35739.
38 M. Khazaei, M. Arai, T. Sasaki, A. Ranjbar, Y. Liang and S. Yunoki, *Phys. Rev. B: Condens. Matter Mater. Phys.*, 2015, **92**, 075411.
39 Y. Liu, H. Xiao and W. A. I. Goddard, *J. Am. Chem. Soc.*, 2016, **138**, 15853–15856.
40 N. M. Caffrey, *Nanoscale*, 2018, **10**, 13520–13530.
41 S. W. Koh, L. Rekhi, Arramel, M. D. Birowosuto, Q. T. Trinh, J. Ge, W. Yu, A. T. S. Wee, T. S. Choksi and H. Li, *ACS Appl. Mater. Interfaces*, 2024, **16**, 66826–66836.
42 K. Yusupov, J. Björk and J. Rosen, *Nanoscale Adv.*, 2023, **5**, 3976–3984.
43 M. Naguib, M. W. Barsoum and Y. Gogotsi, *Adv. Mater.*, 2021, **33**, 2103393.
44 K. R. G. Lim, M. Shekhirev, B. C. Wyatt, B. Anasori, Y. Gogotsi and Z. W. Seh, *Nat. Synth.*, 2022, **1**, 601–614.
45 H. Tang, R. Wang, L. Shi, E. Sheremet, R. D. Rodriguez and J. Sun, *Chem. Eng. J.*, 2021, **425**, 131472.
46 T. Zhang, L. Chang and X. Xiao, *Small Methods*, 2023, 2201530.
47 H. Shi, P. Zhang, Z. Liu, S. Park, M. R. Lohe, Y. Wu, A. Shaygan Nia, S. Yang and X. Feng, *Angew. Chem., Int. Ed.*, 2021, **60**, 8689–8693.
48 M. Li, J. Lu, K. Luo, Y. Li, K. Chang, K. Chen, J. Zhou, J. Rosen, L. Hultman, P. Eklund, P. O. A. Persson, S. Du, Z. Chai, Z. Huang and Q. Huang, *J. Am. Chem. Soc.*, 2019, **141**, 4730–4737.
49 V. Kamysbayev, A. S. Filatov, H. Hu, X. Rui, F. Lagunas, D. Wang, R. F. Klie and D. V. Talapin, *Science*, 2020, **369**, 979–983.
50 T. Zhang, L. Chang, X. Zhang, H. Wan, N. Liu, L. Zhou and X. Xiao, *Nat. Commun.*, 2022, **13**, 6731.
51 H. Ding, Y. Li, M. Li, K. Chen, K. Liang, G. Chen, J. Lu, J. Palisaitis, P. O. A. Persson, P. Eklund, L. Hultman, S. Du, Z. Chai, Y. Gogotsi and Q. Huang, *Science*, 2023, **379**, 1130–1135.
52 M. Shen, W. Jiang, K. Liang, S. Zhao, R. Tang, L. Zhang and J. Wang, *Angew. Chem., Int. Ed.*, 2021, **60**, 27013–27018.
53 I. Persson, J. Halim, H. Lind, T. W. Hansen, J. B. Wagner, L.-Å. Näslund, V. Darakchieva, J. Palisaitis, J. Rosen and P. O. Å. Persson, *Adv. Mater.*, 2019, **31**, 1805472.
54 S. Venkateshalu, M. Shariq, B. Kim, M. Patel, K. S. Mahabari, S.-I. Choi, N. K. Chaudhari, A. N. Grace and K. Lee, *J. Mater. Chem. A*, 2023, **11**, 13107–13132.
55 Y. Georgantas, F. P. Moissinac and M. Bissett, *Graphene 2D Mater.*, 2024, **9**, 5–26.
56 A. Champagne and J.-C. Charlier, *J. Phys. Mater.*, 2021, **3**, 032006.
57 M. Khazaei, A. Ranjbar, M. Arai, T. Sasaki and S. Yunoki, *J. Mater. Chem. C*, 2017, **5**, 2488–2503.
58 U. Yorulmaz, A. Özden, N. K. Perkgöz, F. Ay and C. Sevik, *Nanotechnology*, 2016, **27**, 335702.
59 H. Zhang, G. Yang, X. Zuo, H. Tang, Q. Yang and G. Li, *J. Mater. Chem. A*, 2016, **4**, 12913–12920.
60 K. Luo, X.-H. Zha, Y. Zhou, Q. Huang, S. Zhou and S. Du, *Int. J. Quantum Chem.*, 2020, **120**, e26409.
61 T. Schultz, N. C. Frey, K. Hantanasirisakul, S. Park, S. J. May, V. B. Shenoy, Y. Gogotsi and N. Koch, *Chem. Mater.*, 2019, **31**, 6590–6597.
62 M. López, K. S. Exner, F. Viñes and F. Illas, *Adv. Theory Simul.*, 2022, **2200217**, 1–9.
63 R. Ibragimova, P. Erhart, P. Rinke and H.-P. P. Komsa, *J. Phys. Chem. Lett.*, 2021, **12**, 2377–2384.
64 R. Ibragimova, M. J. Puska and H.-P. Komsa, *ACS Nano*, 2019, **13**, 9171–9181.
65 H. A. Tahini, X. Tan and S. C. Smith, *Nanoscale*, 2017, **9**, 7016–7020.
66 S. Bera and H. Kumar, *J. Phys. Chem. C*, 2023, **127**, 20734–20741.
67 M. Faraji, A. Bafekry, M. M. Fadlallah, F. Molaei, N. N. Hieu, P. Qian, M. Ghergherehchi and D. Gogova, *Phys. Chem. Chem. Phys.*, 2021, **23**, 15319–15328.
68 S. A. Kazemi, S. A. Ogunkunle, O. Allen, W. Wen, A. W.-C. Liew, S. Yin and Y. Wang, *J. Phys. Mater.*, 2023, **6**, 035004.
69 X. Nie, Y. Ji, Y.-M. Ding and Y. Li, *Nanotechnology*, 2023, **34**, 105704.
70 D. Li, X. Chen, P. Xiang, H. Du and B. Xiao, *Appl. Surf. Sci.*, 2020, **501**, 144221.
71 E. Rems, Y.-J. Hu, Y. Gogotsi and R. Dominko, *Chem. Mater.*, 2024, **36**, 10295–10306.
72 J. Björk and J. Rosen, *Chem. Mater.*, 2021, **33**, 9108–9118.
73 J. Yang, A. Wang, S. Zhang, H. Wu and L. Chen, *Comput. Mater. Sci.*, 2018, **153**, 303–308.
74 L. Zhou, Y. Zhang, Z. Zhuo, A. J. Neukirch and S. Tretiak, *J. Phys. Chem. Lett.*, 2018, **9**, 6915–6920.

75 J. Kalmár and F. Karlický, *J. Appl. Phys.*, 2024, **135**, 244302.
76 E. Heidari Semiromi, Z. Khorasani Baghini and A. Mostafaei, *Solid State Commun.*, 2024, **381**, 115451.
77 M.-L. Qin, S.-Y. Wu, T.-H. Guo, M.-Q. Wu, Q.-S. Zhu and M.-Q. Kuang, *Surf. Interfaces*, 2024, **46**, 104073.
78 M. Dahlqvist and J. Rosen, *npj 2D Mater. Appl.*, 2024, **8**, 65.
79 H. Alnoor, A. Elśukova, J. Palisaitis, E. N. Tseng, J. Lu and L. Hultman, *Mater. Today Adv.*, 2021, **9**, 100123.
80 J. D. Gouveia, F. Viñes, F. Illas and J. R. B. Gomes, *Phys. Rev. Mater.*, 2020, **4**, 054003.
81 P. Urbankowski, B. Anasori, T. Makaryan, D. Er, S. Kota, P. L. Walsh, M. Zhao, V. B. Shenoy, M. W. Barsoum and Y. Gogotsi, *Nanoscale*, 2016, **8**, 11385–11391.
82 E. B. Deeva, A. Kurlov, P. M. Abdala, D. Lebedev, S. M. Kim, C. P. Gordon, A. Tsoukalou, A. Fedorov and C. R. Müller, *Chem. Mater.*, 2019, **31**, 4505–4513.
83 Y. Kong, S. Yan, J. Feng, S. Wang and H. Pan, *J. Mater. Chem. A*, 2021, **9**, 597–606.
84 J. D. Gouveia and J. R. B. Gomes, *Phys. Rev. Mater.*, 2022, **6**, 024004.
85 A. Jurado, Á. Morales-García, F. Viñes and F. Illas, *J. Phys. Chem. C*, 2021, **125**, 26808–26813.
86 G. Kresse and J. Hafner, *Phys. Rev. B: Condens. Matter Mater. Phys.*, 1994, **49**, 14251–14269.
87 G. Kresse and J. Hafner, *Phys. Rev. B: Condens. Matter Mater. Phys.*, 1993, **47**, 558–561.
88 G. Kresse and J. Furthmüller, *Phys. Rev. B: Condens. Matter Mater. Phys.*, 1996, **54**, 11169–11186.
89 G. Kresse and J. Furthmüller, *Comput. Mater. Sci.*, 1996, **6**, 15–50.
90 J. P. Perdew, K. Burke and M. Ernzerhof, *Phys. Rev. Lett.*, 1996, **77**, 3865–3868.
91 P. E. Blöchl, *Phys. Rev. B: Condens. Matter Mater. Phys.*, 1994, **50**, 17953–17979.
92 G. Kresse and D. Joubert, *Phys. Rev. B: Condens. Matter Mater. Phys.*, 1999, **59**, 1758–1775.
93 J. Heyd, G. E. Scuseria and M. Ernzerhof, *J. Chem. Phys.*, 2003, **118**, 8207–8215.
94 V. Wang, N. Xu, J.-C. Liu, G. Tang and W.-T. Geng, *Comput. Phys. Commun.*, 2021, **267**, 108033.
95 G. Henkelman, A. Arnaldsson and H. Jónsson, *Comput. Mater. Sci.*, 2006, **36**, 354–360.
96 V. Wang, G. Tang, Y. C. Liu, R. T. Wang, H. Mizuseki, Y. Kawazoe, J. Nara and W. T. Geng, *J. Phys. Chem. Lett.*, 2022, **13**, 11581–11594.
97 B. Hammer and J. K. Nørskov, *Surf. Sci.*, 1995, **343**, 211–220.
98 J. R. Kitchin, J. K. Nørskov, M. A. Barteau and J. G. Chen, *J. Chem. Phys.*, 2004, **120**, 10240–10246.
99 M. Gajdo, A. Eichler and J. Hafner, *J. Phys.: Condens. Matter*, 2004, **16**, 1141–1164.
100 B. S. Mun, M. Watanabe, M. Rossi, V. Stamenkovic, N. M. Markovic and P. N. Ross, *J. Chem. Phys.*, 2005, **123**, 204717.
101 T. Hofmann, T. H. Yu, M. Folse, L. Weinhardt, M. Bär, Y. Zhang, B. V. Merinov, D. J. Myers, W. A. Goddard and C. Heske, *J. Phys. Chem. C*, 2012, **116**, 24016–24026.
102 K. Momma and F. Izumi, *J. Appl. Crystallogr.*, 2008, **41**, 653–658.
103 *mendeleev – A Python resource for properties of chemical elements, ions and isotopes, ver. 1.0.0*, 2014, **https://github.com/lmmentel/mendeleev**.
104 J. Demšar, T. Curk, A. Erjavec, Črt Gorup, T. Hočevar, M. Milutinovič, M. Možina, M. Polajnar, M. Toplak, A. Starič, M. Štajdohar, L. Umek, L. Žagar, J. Žbontar, M. Žitnik and B. Zupan, *J. Mach. Learn. Res.*, 2013, **14**, 2349–2353.
105 Y. Li, H. Shao, Z. Lin, J. Lu, L. Liu, B. Duployer, P. O. A. Persson, P. Eklund, L. Hultman, M. Li, K. Chen, X.-H. Zha, S. Du, P. Rozier, Z. Chai, E. Raymundo-Pñero, P.-L. Taberna, P. Simon and Q. Huang, *Nat. Mater.*, 2020, **19**, 894–899.
106 M. Kertesz and R. Hoffmann, *J. Am. Chem. Soc.*, 1984, **106**, 3453–3460.
107 A. Miura, K. Tadanaga, E. Magome, C. Moriyoshi, Y. Kuroiwa, T. Takahiro and N. Kumada, *J. Solid State Chem.*, 2015, **229**, 272–277.
108 D. R. Askeland and W. Wright, *The science and engineering of materials*, CENGAGE Learning Custom Publishing, Mason, OH, 7th edn, 2015.
109 T. Sato, S. Takagi, S. Deledda, B. C. Hauback and S.-I. Orimo, *Sci. Rep.*, 2016, **6**, 23592.
110 Z. Yang, Y. Zheng, W. Li and J. Zhang, *J. Comput. Chem.*, 2019, **40**, 1352–1359.
111 Y. Shao, F. Zhang, X. Shi and H. Pan, *Phys. Chem. Chem. Phys.*, 2017, **19**, 28710–28717.
112 M. Naguib, M. Kurtoglu, V. Presser, J. Lu, J. Niu, M. Heon, L. Hultman, Y. Gogotsi and M. W. Barsoum, *Adv. Mater.*, 2011, **23**, 4248–4253.
113 T. Hu, Z. Li, M. Hu, J. Wang, Q. Hu, Q. Li and X. Wang, *J. Phys. Chem. C*, 2017, **121**, 19254–19261.
114 N. Zhang, Y. Hong, S. Yazdanparast and M. Asle Zaeem, *2D Mater.*, 2018, **5**, 045004.
115 Y. Xin and Y.-X. Yu, *Mater. Des.*, 2017, **130**, 512–520.
116 P. Roy, L. Rekhi, S. W. Koh, H. Li and T. S. Choksi, *JPhys Energy*, 2023, **5**, 034005.
117 Q. Zhu and S.-q Wang, *J. Electrochem. Soc.*, 2016, **163**, H796–H808.
118 F. Gossenberger, T. Roman, K. Forster-Tonigold and A. Groß, *Beilstein J. Nanotechnol.*, 2014, **5**, 152–161.
119 F. Gossenberger, T. Roman and A. Groß, *Surf. Sci.*, 2015, **631**, 17–22.
120 R. Jacobs, J. Booske and D. Morgan, *Adv. Funct. Mater.*, 2016, **26**, 5471–5482.
121 T. C. Leung, C. L. Kao, W. S. Su, Y. J. Feng and C. T. Chan, *Phys. Rev. B: Condens. Matter Mater. Phys.*, 2003, **68**, 68–73.
122 J. M. Crowley, J. Tahir-Kheli and W. A. Goddard, *J. Phys. Chem. Lett.*, 2016, **7**, 1198–1203.
123 H.-D. Saßnick and C. Cocchi, *Electron. Struct.*, 2021, **3**, 027001.
124 E. M. Flores, M. L. Moreira and M. J. Piotrowski, *J. Phys. Chem. A*, 2020, **124**, 3778–3785.
125 Y. X. Wang, H. Y. Geng, Q. Wu and X. R. Chen, *J. Chem. Phys.*, 2020, **152**, 024118.

126 T. M. Henderson, J. Paier and G. E. Scuseria, *Phys. Status Solidi B*, 2010, **248**, 767–774.
127 W. Gao, T. A. Abtew, T. Cai, Y.-Y. Sun, S. Zhang and P. Zhang, *Solid State Commun.*, 2016, **234–235**, 10–13.
128 K. Pokharel, C. Lane, J. W. Furness, R. Zhang, J. Ning, B. Barbiellini, R. S. Markiewicz, Y. Zhang, A. Bansil and J. Sun, *npj Comput. Mater.*, 2022, **8**, 31.
129 Y. Meng, X.-W. Liu, C.-F. Huo, W.-P. Guo, D.-B. Cao, Q. Peng, A. Dearden, X. Gonze, Y. Yang, J. Wang, H. Jiao, Y. Li and X.-D. Wen, *J. Chem. Theory Comput.*, 2016, **12**, 5132–5144.
130 S. S. Li, *Semiconductor physical electronics*, Springer Science & Business Media, 2012.
131 A. C. Rajan, A. Mishra, S. Satsangi, R. Vaish, H. Mizuseki, K.-R. R. Lee and A. K. Singh, *Chem. Mater.*, 2018, **30**, 4031–4038.
132 K. Hantanasirisakul and Y. Gogotsi, *Adv. Mater.*, 2018, **30**, 1–30.
133 B. Ul Haq, S.-H. Kim, I. Khadka, R. Ahmed, S. AlFaify, A. R. Chaudhry and Y. A. Obaidat, *Emergent Mater.*, 2023, **6**, 1991–1999.
134 Y.-m Ding, X. Nie, H. Dong, N. Rujisamphan and Y. Li, *Nanoscale Adv.*, 2020, **2**, 2471–2477.
135 A. Patra, S. Jana, P. Samal, F. Tran, L. Kalantari, J. Doumont and P. Blaha, *J. Phys. Chem. C*, 2021, **125**, 11206–11215.
136 Y. Zhang, M. Wu, Z. Wang, N. Zhang and C. Ge, *J. Mater. Res.*, 2021, **36**, 1678–1685.
137 X.-H. Zha, J. Zhou, K. Luo, J. Lang, Q. Huang, X. Zhou, J. S. Francisco, J. He and S. Du, *J. Phys.: Condens. Matter*, 2017, **29**, 165701.
138 N. Kumar, M. Kolos, S. Bhattacharya and F. Karlický, *J. Chem. Phys.*, 2024, **160**, 124707.
139 S. Qiao, Y. Zhang, S. Li, L. Wei, H. Wu and F. Li, *Phys. Chem. Chem. Phys.*, 2025, **27**, 513–519.
140 Y. Xie and P. R. C. Kent, *Phys. Rev. B: Condens. Matter Mater. Phys.*, 2013, **87**, 235441.
141 K. A. Papadopoulou, A. Chroneos, D. Parfitt and S.-R. G. Christopoulos, *J. Appl. Phys.*, 2020, **128**, 170902.
142 W. Zheng, B. Sun, D. Li, S. M. Gali, H. Zhang, S. Fu, L. Di Virgilio, Z. Li, S. Yang, S. Zhou, D. Beljonne, M. Yu, X. Feng, H. I. Wang and M. Bonn, *Nat. Phys.*, 2022, **18**, 544–550.
143 P. Eliášová, B. Šmíd, J. Vejpravová, S. Li, F. Brivio, M. Mazur, D. N. Rainer, M. I. H. Mohideen, R. E. Morris and P. Nachtigall, *J. Mater. Chem. C*, 2024, **12**, 5431–5441.
144 J. Hart, K. Hantanasirisakul, A. C. Lang, B. Anasori, D. Pinto, Y. Pivak, J. Tijn van Omme, S. J. May, Y. Gogotsi and M. L. Taheri, *Nat. Commun.*, 2019, **10**, 1–10.
145 R. Khanal and S. Irle, *J. Chem. Phys.*, 2023, **158**, 194701.
146 J. Fatima, M. Tahir, A. Rehman, M. Sagir, M. Rafique, M. A. Assiri, M. Imran and M. Alzaid, *Mater. Sci. Eng. B*, 2023, **289**, 116230.
147 N. Zhang, Y. Hong, S. Yazdanparast and M. Asle Zaeem, *2D Mater.*, 2018, **5**, 045004.
148 G. Bharathi and S. Hong, *Materials*, 2024, **18**, 104.
149 B. Hammer and J. Nørskov, *Impact of Surf. Sci. on Catalysis*, Academic Press, 2000, vol. 45, pp. 71–129.
150 Y. Guan, Y. Cong, R. Zhao, K. Li, X. Li, H. Zhu, Q. Zhang, Z. Dong and N. Yang, *Small*, 2023, **19**, 2301276.
151 Y. Wang, J. Fu, H. Hu and D. Ho, *ACS Appl. Mater. Interfaces*, 2023, **15**, 40846–40854.
152 Y. Zhang, Y. Wang, N. Ma, B. Liang, Y. Xiong and J. Fan, *Small*, 2024, **20**, 2306840.
153 P. Liu, H. Xu, X. Wang, G. Tian, X. Wen, C. Wang, C. Zeng, S. Wang, F. Fan and T. Zeng, *et al.*, *J. Colloid Interface Sci.*, 2024, **655**, 364–370.
154 Z. Wang, Z. Dong, B. Wu, Z. Wang, Z. Qiu, D. Wang, Q. Zeng, X. Liu, K. Nam Hui, Z. Liu and Y. Zhang, *J. Colloid Interface Sci.*, 2024, **676**, 368–377.
155 F. Mouhat and F.-X. Coudert, *Phys. Rev. B: Condens. Matter Mater. Phys.*, 2014, **90**, 224104.
156 K. Liu and J. Wu, *J. Mater. Res.*, 2015, **31**, 832–844.
157 A. V. Dyskin, E. Pasternak and Y. Xu, *Phys. Status Solidi B*, 2017, **254**, 1600851.
158 S. Xinchun and R. S. Lakes, *Phys. Status Solidi B*, 2007, **244**, 1008–1026.
159 D. Wu, S. Wang, S. Zhang, J. Yuan, B. Yang and H. Chen, *Phys. Chem. Chem. Phys.*, 2018, **20**, 18924–18930.
160 B. Mortazavi, M. Shahrokhi, M. Makaremi and T. Rabczuk, *Nanotechnology*, 2017, **28**, 115705.
161 X. Du, J. Zhao, J. Wang, X. Liu, Z. Ye, L. Fang and M. Zhou, *J. Chem. Phys.*, 2025, **162**, 014703.
162 C. Huang and L. Chen, *Adv. Mater.*, 2016, **28**, 8079–8096.
163 G. Qin and Z. Qin, *Npj Comput. Mater.*, 2020, **6**, 51.
164 P. Schindler, E. R. Antoniuk, G. Cheon, Y. Zhu and E. J. Reed, *Adv. Funct. Mater.*, 2024, **34**, 2401764.
165 Y. Li, F. Liu, Z. Sui and C. Jiang, *Thin Solid Films*, 2022, **741**, 139038.
166 S. Ahn, T. Han, K. Maleski, J. Song, Y. Kim, M. Park, H. Zhou, S. Yoo, Y. Gogotsi and T. Lee, *Adv. Mater.*, 2020, **32**, 2000919.
167 P. Lu, J. Wu, X. Shen, X. Gao, Z. Shi, M. Lu, W. W. Yu and Y. Zhang, *Adv. Sci.*, 2020, **7**, 2001562.
168 S. Chuang, C. Battaglia, A. Azcatl, S. McDonnell, J. S. Kang, X. Yin, M. Tosun, R. Kapadia, H. Fang, R. M. Wallace and A. Javey, *Nano Lett.*, 2014, **14**, 1337–1342.
169 B. Lyu, M. Kim, H. Jing, J. Kang, C. Qian, S. Lee and J. H. Cho, *ACS Nano*, 2019, **13**, 11392–11400.
170 J. You, C. Si, J. Zhou and Z. Sun, *J. Phys. Chem. C*, 2019, **123**, 3719–3726.
171 S. Qamar, K. Fatima, N. Ullah, Z. Akhter, A. Waseem and M. Sultan, *Nanoscale*, 2022, **14**, 13018–13039.
172 J. Zhang, C. Huang and H. Yu, *Appl. Phys. Lett.*, 2021, **119**, 033506.
173 Z. Yu, W. Feng, W. Lu, B. Li, H. Yao, K. Zeng and J. Ouyang, *J. Mater. Chem. A*, 2019, **7**, 11160–11169.
174 N. U. Kiran, A. B. Deore, M. A. More, D. J. Late, C. S. Rout, P. Mane, B. Chakraborty, L. Besra and S. Chatterjee, *ACS Appl. Electron. Mater.*, 2022, **4**, 2656–2666.
175 J. Chen, B. Yang, Y. D. Lim, W. Duan, Y. Zhao, B. K. Tay and X. Yan, *Nanotechnology*, 2020, **31**, 285701.

176 S. Yamamoto, *Appl. Surf. Sci.*, 2005, **251**, 4–13.
177 C. Peng, P. Wei, X. Li, Y. Liu, Y. Cao, H. Wang, H. Yu, F. Peng, L. Zhang, B. Zhang and K. Lv, *Nano Energy*, 2018, **53**, 97–107.
178 M. Li, B. Cai, R. Tian, X. Yu, M. B. Breese, X. Chu, Z. Han, S. Li, R. Joshi, A. Vinu, T. Wan, Z. Ao, J. Yi and D. Chu, *Chem. Eng. J.*, 2021, **409**, 128158.
179 A. Sherryna and M. Tahir, *ACS Appl. Energy Mater.*, 2021, **4**, 11982–12006.
180 R. Jacobs, D. Morgan and J. Booske, *APL Mater.*, 2017, **5**, 116105.
181 T. Ma, R. Jacobs, J. Booske and D. Morgan, *J. Mater. Chem. C*, 2021, **9**, 12778–12790.
182 M. Khazaei, M. Arai, T. Sasaki, M. Estili and Y. Sakka, *Phys. Chem. Chem. Phys.*, 2014, **16**, 7841–7849.
183 M. P. Bilibana, *AdSEM*, 2023, **2**, 100080.
184 B. Miao, T. Bashir, H. Zhang, T. Ali, S. Raza, D. He, Y. Liu and J. Bai, *Renewable Sustainable Energy Rev.*, 2024, **199**, 114506.
185 Y. Huang, S. Jiang, R. Liang, P. Sun, Y. Hai and L. Zhang, *Chem. Eng. J.*, 2020, **391**, 123621.
186 W. Chen, X. Song, X. He, Y. Su, S.-K. Oh, S. Chen and Q. Sun, *Prog. Org. Coat.*, 2024, **186**, 108021.
187 D. An, Z. Wang, L. Qin, Y. Wu, S. Lu, H. Yang, Z. Ma, F. J. Mawignon, J. Liu, L. Hao and G. Li, *Prog. Org. Coat.*, 2023, **183**, 107779.
188 A. Maleki, M. Ghomi, N. Nikfarjam, M. Akbari, E. Sharifi, M. Shahbazi, M. Kermanian, M. Seyedhamzeh, E. Nazarzadeh Zare, M. Mehrali, O. Moradi, F. Sefat, V. Mattoli, P. Makvandi and Y. Chen, *Adv. Funct. Mater.*, 2022, **32**, 2203430.
189 H. Huang, C. Dong, W. Feng, Y. Wang, B. Huang and Y. Chen, *Adv. Drug Delivery Rev.*, 2022, **184**, 114178.
190 S. Iravani, E. Nazarzadeh Zare and P. Makvandi, *ACS Biomater. Sci. Eng.*, 2024, **10**, 1892–1909.
191 M. Malaki and R. S. Varma, *Adv. Mater.*, 2020, **32**, 2003154.
192 Y. Sliozberg, J. Andzelm, C. B. Hatter, B. Anasori, Y. Gogotsi and A. Hall, *Compos. Sci. Technol.*, 2020, **192**, 108124.
193 J. Hu, S. Li, J. Zhang, Q. Chang, W. Yu and Y. Zhou, *Chin. Chem. Lett.*, 2020, **31**, 996–999.
194 R. Chen, X. Xu, D. Yu, C. Xiao, M. Liu, J. Huang, T. Mao, C. Zheng, Z. Wang and X. Wu, *J. Mater. Chem. C*, 2018, **6**, 11193–11201.
195 D. Yu, Y. Teng, N. Zhou, Y. Xu, X. Wang, X. Lin, Q. Wang and C. Xue, *Colloids Surf., A*, 2023, **659**, 130752.
196 M. Xin, J. Li, Z. Ma, L. Pan and Y. Shi, *Front. Chem.*, 2020, **8**, DOI: 10.3389/fchem.2020.00297.
197 K. K. Saxena, R. Das and E. P. Calius, *Adv. Eng. Mater.*, 2016, **18**, 1847–1870.
198 D. Wang, C. Zhou, A. S. Filatov, W. Cho, F. Lagunas, M. Wang, S. Vaikuntanathan, C. Liu, R. F. Klie and D. V. Talapin, *Science*, 2023, **379**, 1242–1247.